1 **Bmper is required for morphogenesis of the anterior and posterior semicircular canal**

2 **ducts in the developing zebrafish inner ear**

3 Sarah Baxendale[1], Esther C. Maier[1,a], Nikolaus D. Obholzer[2], Sarah Burbridge[1], Joseph

4 Zinski[3], Francesca B. Tuazon[3], Nicholas J. van Hateren[1], M. Montserrat Garcia Romero[1],

5 Mar Marzo[1], Kazutomo Yokoya[4], Robert D. Knight[4], Sean G. Megason[2], Mary C. Mullins[3]

6 and Tanya T. Whitfield[1,#]

7 [#]Corresponding author: t.whitfield@sheffield.ac.uk

8 Key words: *bmper, Cv-2, dlx5a, smad6b*, BMP signalling, zebrafish, inner ear, semicircular

9 canals, neural crest, otic placode

10 [1]Department of Biomedical Science and Bateson Centre, University of Sheffield, Sheffield,

11 S10 2TN, UK

12 [2]Department of Systems Biology, Harvard Medical School, 200 Longwood Avenue, Boston

13 MA 02115, USA

14 [3]Department of Cell and Developmental Biology, University of Pennsylvania, Perelman

15 School of Medicine, Philadelphia, USA

16 [4]Centre for Craniofacial and Regenerative Biology, King's College London, Guy's Hospital,

17 London SE1 9RT, UK

18

19 Current address:

20 [a]Research Group Anatomy, School of Medicine and Health Sciences, Carl von Ossietzky

21 University Oldenburg, D-26129 Oldenburg, Germany

22

23

24 ORCID:

25 Sarah Baxendale 0000-0002-6760-9457

26 Nicholas J. van Hateren 0000-0002-0011-9947

27 Mar Marzo 0000-0003-1591-0309

28 Tanya T. Whitfield 0000-0003-1575-1504

29 Robert D. Knight 0000-0001-9920-836X

30

31

32   **Summary**

33   BMP signalling is known to have a conserved function in development of the semicircular

34   canal system of the vertebrate inner ear, but its regulation, target genes and effects on cell

35   behaviour during otic morphogenesis are not fully understood. We have characterised the

36   effects of mutations in the zebrafish gene *bmper,* which codes for a regulator of BMP

37   signalling with both pro- and anti-BMP roles in different developmental contexts. The inner

38   ears of *bmper* mutant embryos develop with truncations of the anterior and posterior

39   semicircular canal ducts. To image the developing ear in live embryos, we have exploited a

40   new transgenic line, *Tg(smad6b:EGFP)*, which exhibits strong GFP expression in the otic

41   epithelium. Morphometric analysis indicates defects in the *bmper* mutant ear from early

42   stages of semicircular canal formation, correlating with a specific reduction in BMP signalling

43   activity and specific loss of *dlx5a* expression in dorsal otic epithelium. Subsequent changes

44   to cell shape occur at the truncation site and the dorsolateral septum. The *bmper* mutations

45   that we describe are adult viable; truncation of the anterior and posterior semicircular canal

46   ducts persists into adulthood. Our results argue against a major role for Bmper in

47   specification of the pre-placodal region, induction of the otic placode, or development of the

48   neural crest, processes in which Bmper function has previously been implicated. Instead,

49   we conclude that a key requirement for Bmper function in the zebrafish is to promote BMP

50   signalling during patterning and morphogenesis of the semicircular canal system.

51

Introduction

Formation of the interlinked ducts and chambers that make up the semicircular canal system of the vertebrate inner ear is a spectacular example of epithelial morphogenesis in the developing embryo (reviewed in Alsina and Whitfield, 2017). BMP signalling is known to play an important role in otic patterning and morphogenesis at multiple stages of ear development, including in formation of the semicircular canal system. At gastrula stages, a dorsal (low)-to-ventral (high) gradient of BMP signalling activity patterns the dorsoventral axis of the entire embryo, a process that contributes to the positioning of the preplacodal region (PPR) and neural crest at the border between the neural plate and non-neural ectoderm (Nguyen et al., 1998; Tuazon and Mullins, 2015). The PPR gives rise to all cranial sensory placodes, including the otic placode, precursor of the inner ear. Correct PPR specification and placode induction involves modification of the BMP gradient; specifically, BMP signalling must be attenuated for otic placode induction within the PPR (Bhat et al., 2013; Reichert et al., 2013; reviewed in Groves and LaBonne, 2014).

After otic vesicle formation, genes coding for BMPs, BMP receptors and BMP signalling modulators show conserved patterns of expression in the developing ear, including in the semicircular canals and their associated sensory cristae (Chang et al., 2002; Chang et al., 2004; Morsli et al., 1998; Mowbray et al., 2001; Oh et al., 1996; Shawi and Serluca, 2008; Wu and Oh, 1996). In zebrafish, both *bmp2b* and *bmp4* are expressed at the anterior and posterior of the otic vesicle at 24 hours post fertilisation (hpf), and later in the developing cristae; *bmp7a* is expressed in the posterior of the otic vesicle, whereas *bmp7b* is expressed later in the outgrowing epithelial projections that fuse to form pillars of tissue (the hubs of the canal ducts) spanning the otic lumen, becoming down-regulated on fusion (Mowbray et al., 2001; Schmid et al., 2000; Shawi and Serluca, 2008). At least five genes coding for antagonists or modulators of BMP signalling (*bmper*, *fsta*, *chordin*, *smad6a*, and *smad6b*) are also expressed in or around the developing zebrafish ear (Esterberg and Fritz, 2009; Hammond and Whitfield, 2006; Kudoh et al., 2001; Mowbray et al., 2001). A transgenic reporter of BMP activity reveals expression in the otic vesicle, in a similar pattern to that of *bmp2b* at 24 hpf (Collery and Link, 2011).

As BMP signalling plays a central role in dorsoventral axial patterning of the embryo during early development, leading to embryonic lethal phenotypes for mutations in several BMP pathway genes, conditional approaches have been employed to study its function during inner ear morphogenesis. In the zebrafish, loss of *bmp2b* function during larval stages, following RNA-mediated rescue of embryonic axial patterning in *bmp2b* mutants, resulted in a complete absence of all three semicircular canal ducts in the adult ear, although ampullae,

87   sensory cristae and the crus commune were present. These *bmp2b* mutant fish also

88   displayed an abnormal swimming behaviour, indicative of balance defects (Hammond et al.,

89   2009). In the mouse, conditional loss of *Bmp4* led to a loss of all three cristae and

90   semicircular canal ducts in the most severe cases (Chang et al., 2008), and conditional

91   inactivation of the *Alk3* type I BMP receptor gene in an *Alk6+/-* background resulted in thin or

92   truncated canals (Ohyama et al., 2010). In chick, application or mis-expression of the BMP

93   antagonists Noggin, DAN or Smad6 resulted in malformed or missing cristae and canals

94   (Chang et al., 1999; Chang et al., 2008; Gerlach-Bank et al., 2004; Gerlach et al., 2000;

95   Ohta et al., 2010). BMP signalling has been shown to drive the epithelial thinning that forms

96   the dorsolateral pouch (precursor of the anterior and posterior semicircular canal ducts)

97   (Ohta et al., 2010), and is thought to work via both canonical (SMAD-dependent) and non-

98   canonical (PKA-dependent) pathways to regulate expression of *Dlx5* and *Hmx3*,

99   respectively, in the chick otic vesicle (Ohta et al., 2016).

100 In this paper, we identify and characterise recessive mutations in the zebrafish *BMP-binding*

101 *endothelial regulator* (*bmper*) gene, which codes for a BMP regulator and is itself

102 transcriptionally responsive to BMP signalling. The zygotic *bmper* mutant displays very

103 specific and fully penetrant but variably expressive defects in the inner ear, leading to

104 truncations of the anterior and posterior semicircular canal ducts. We have imaged the otic

105 phenotype using a new transgenic line, *Tg*(*smad6b:EGFP*), which provides a live readout for

106 the expression of *smad6b*, a BMP inhibitor gene. Based on transcriptional changes and a

107 reduction in BMP pathway activity in the *bmper* mutant ear, we propose a pro-BMP role for

108 Bmper in dorsal otic epithelium, with *dlx5a* as a target gene. Both zygotic and most

109 maternal-zygotic (MZ) *bmper* mutants are adult viable and fertile; we did not find any major

110 defects in embryonic development of the neural crest or cardiovascular systems, tissues in

111 which a role for Bmper has previously been suggested. Our work confirms the importance

112 of BMP signalling in formation of the vertebrate semicircular canal system, and identifies

113 Bmper as a key regulatory BMP-promoting factor in zebrafish dorsal otic morphogenesis.

114

Materials and Methods

Animals

Zebrafish lines used were AB, London wild type (LWT), King's College wild type (KWT), *bmper^sa108^*, *bmper^del2^*, *bmper^del5^* (this work), *Tg(Xla.Eef1a1:h2b-mRFP1)* (Rodríguez-Aznar et al., 2013), *Tg(smad6b:EGFP-CAAX)* (this work) and *Tg(BMPRE:mRFP)* (Reichert et al., 2013). All mutants described are homozygous for the zygotic allele, except where maternal-zygotic (MZ) mutants were used, as indicated. Animals were maintained according to recommended husbandry regulations (Aleström et al., 2020), and all animal experiments conformed to UK Home Office or US regulations.

Generation of the *Tg(smad6b:EGFP-CAAX)* line

The *Tg(smad6b:EGFP-CAAX)* line (referred to throughout as *Tg(smad6b:EGFP)*) was generated in an enhancer trap screen by ligating a 4.1 kb fragment upstream of the zebrafish *en2a* coding region to a minimal *c-fos* promoter driving membrane-(CAAX)-tagged EGFP in the Gateway vector pDestTol2. The construct was injected into the KWT strain using the Tol2 system (Kawakami, 2007). Injected embryos were grown up to adulthood and their offspring selected on the basis of GFP expression in the ear. Transgenic individuals were crossed to the *bmper^sa108^* line for imaging the otic epithelium.

Identification of the *Tg(smad6b:EGFP)* line insertion site

Two methods were used to identify the insertion site of the transgene (Supplementary Figure S2). Thermal asymmetric interlaced (TAIL)-PCR (Liu and Whittier, 1995; Parinov et al., 2004), which alternates a higher annealing temperature for the specific Tol2 transgene primers, and a lower annealing temperature for degenerate primers to bind to the genomic sequence, was used to generate short fragments flanking the transgene insertion site. TAIL-PCR products from the secondary and tertiary nested PCR reactions were separated by gel electrophoresis, and fragments with the correct size shift—corresponding to the distance between the nested Tol2 primer sites—were isolated and sequenced. Tol2 and degenerate (AD) primer sequences used were: Tol2 5′-1, GGGAAAATAGAATGAAGTGATCTCC, Tol2 5′-2 GACTGTAAATAAAATTGTAAGGAG, Tol2 5′-3 CCCCAAAAATAATACTTAAGTACAG, Tol2 3′-1 CTCAAGTACAATTTTAATGGAGTAC, Tol2 3′-2 ACTCAAGTAAGATTCTAGCCAGA, Tol2 3′-3 CCTAAGTACTTGTACTTTCACTTG, AD-3 WGTGNAGNANCANAGA, AD-5 WCAGNTGWTNGTNCTG, AD-6 STTGNTASTNCTNTGC, AD-11 NCASGAWAGNCSWCAA.

Sequences from either side of the insertion site were mapped to the zebrafish GRCz11 genome assembly and two fragments (Tol2 5′-3/AD11 and Tol2 3′-3/AD5) identified the

5

149   same locus at Ch18:19,713,380 (GRCz11) at the 3' end of the *smad6b* locus. This insertion

150   site was confirmed using the Targeted Locus Amplification (TLA) method (Cergentis B.V.,

151   Utrecht, Netherlands, (De Vree et al., 2014; Hottentot et al., 2017). For cell preparation, the

152   protocol was adapted for use with zebrafish as follows (see Supplementary Fig. S2). Two

153   hundred zebrafish embryos at the 15-20 somite stage were dissociated in a clean Petri dish

154   under a coverslip in a minimal volume of calcium-free Ringer's solution, as previously

155   described (Baxendale et al., 2009). Cells were collected in a 1.5 ml reaction tube and

156   separated from yolk platelets by centrifugation at 300g for 1 minute. The pellet of embryo

157   cells was gently resuspended in Accumax cell dissociation medium and incubated until cells

158   were fully dissociated. DNA crosslinking using ~10^7 cells and the Cergentis kit were used to

159   fix the cells before being shipped to Cergentis B.V. for TLA analysis.

160   Two integration sites were found: one at Ch18:19,713,380 (GRCz11), corresponding to the

161   *smad6b* locus, and a second insertion site at Ch16:50,170,719 (GRCz11) within the

162   *cysteine-rich venom protein natrin-1-like* (*crvpn1l*) gene. Both insertion sites were confirmed

163   by PCR using genome-specific primers to either side of the insertion: *smad6b* locus: F:

164   GGGTTAGGGGTAGGAAAGGAATA, R: GCAAACATACCCACGTTGCTAT, *crvpn1l* locus:

165   F: GGACATATCACCTAAATCCGCTG, R: GTACAATAAATACACCTCAATG.

Mapping and identification of the genetic lesion using RNAseq and RNAmapper

167   To map and identify the *bmper* mutation, we followed the RNAmapper pipeline

168   (http://www.rnamapper.org/) (Miller et al., 2013). In brief, mRNA was isolated from *bmper*

169   mutant and sibling larvae at 3 days post fertilisation (dpf), sorted by ear phenotype into

170   separate pools of 35 larvae each. Each pool was then sequenced to approximately 5 million

171   PE76 reads on a HiSeq2000 machine, covering 61.7% of the transcriptome (Zv9.65) >4-fold.

172   We obtained coverage for >95% of genes, with an average coverage of 26 reads per

173   position. Sequencing reads were entered into the RNAmapper pipeline in FASTQ format.

174   Based on de novo SNPs, RNAmapper predicted that the mutation lay within a 13.9 Mb

175   interval on chromosome 16 (chr16: 1,444,165-15,420,254; peak AF: 0.951). Within the

176   critical interval, we detected four candidate genes with potentially serious deleterious

177   changes: *foxo6*, *stx12l*, *bmper* and *ptpn2a*.

178   Based on the known expression pattern of *bmper* in the otic vesicle and the known

179   conserved role of BMP signalling in otic development, we prioritised *bmper* and confirmed a

180   G>A transition mutation at 16:9261799 (Chromosome 16: 7,154,266-7,195,000 on GRCz11)

181   by RT-PCR and sequencing.

TALEN mutagenesis

183   TALEN targeted mutagenesis was used to create a 2 bp and 5 bp deletion at 669/2004

184   (223/668aa) in exon 8 of the 16-exon transcript (ENSDARG00000040893) (Fig. 3).

In situ hybridisation and Immunohistochemistry

186   in situ hybridisation was performed as previously described (Oxtoby and Jowett, 1993;

187   Thisse and Thisse, 2008). Probes used are listed in Supplementary Table S1. Whole

188   embryos were fixed in 4% paraformaldehyde overnight and stained with anti-phospho-

189   Smad1/5/9 Rabbit monoclonal antibody (Cell Signaling Technology #13820S; 1:500), anti-

190   phospho-H3 Rabbit monoclonal antibody (Cell Signaling Technology #9701S; 1:500),

191   followed by Goat anti-Rabbit Alexa 568 secondary antibody (1:200).

Alcian blue staining

193   Craniofacial cartilages were stained using the alcian blue method, as previously described

194   for zebrafish (Felber et al., 2015).

Imaging

196   Fixed embryos stained by in situ hybridisation or with alcian blue were imaged on an

197   Olympus BX51 compound microscope equipped with DIC optics, a Camedia C-3030ZOOM

198   camera and CELL-B software. For Figures S4, 5 and 6, batches of embryos from a mixed

199   cross of homozygous and heterozygous *bmper* mutant fish, with an expected ratio of 50:50,

200   homozygous mutant:heterozygous sibling, were used. >30 embryos were analysed with

201   each probe and at each stage of development. Fluorescent antibody stains were imaged on

202   an Olympus FV-1000 confocal microscope. Live transgenic embryos were anaesthetised in

203   0.5 mM MS222 (3-aminobenzoic acid ethyl ester) and mounted in 3% methylcellulose or in

204   0.7% agarose for imaging with a 20× objective on an Olympus FV-1000 confocal microscope

205   or a Zeiss Z.1 light-sheet microscope. Light-sheet datasets were analysed in Zen black

206   (Zeiss) or arivis software. Fiji (Schindelin et al., 2012) or Adobe Photoshop were used to

207   adjust brightness and contrast. Levels of P Smad5 staining in Fig. 5 were quantified as

208   previously described (Zinski et al., 2019).

Adult ear dissections and TRITC-phalloidin staining

210   Adult zebrafish were killed with an overdose of MS222 (3-aminobenzoic acid ethyl ester) and

211   decapitated. Heads were fixed in 4% paraformaldehyde for at least 1 week. Ears were

212   dissected and stained with TRITC-phalloidin (Sigma) as previously described (Baxendale

213   and Whitfield, 2016). The image shown in Fig. 7G appeared in this publication.

Data Analysis

215   Statistical analyses were performed using GraphPad Prism version 9.

7

216 **Results**

217 **The zebrafish *bmper* mutant ear has truncated anterior and posterior semicircular**

218 **canal ducts**

219 We identified a recessive mutation affecting ear morphology in the background of the

220 zebrafish *otx1b*^{sa96} line, obtained from the Sanger Centre Zebrafish Mutation Project

221 (Kettleborough et al., 2013). The mutation, named *bmper* following the identification of the

222 genetic lesion (see below), results in a truncation of the anterior and posterior semicircular

223 canal ducts, with defects visible under the dissecting microscope from around 52 hours post

224 fertilisation (hpf). Other structures in the ear, including the otoliths, all three semicircular

225 canal cristae and the lateral (horizontal) semicircular canal duct, appear to develop normally

226 (Fig. 1A, Supplementary Movies 1-3). The epithelial projections that meet and fuse to form

227 the pillars around which the anterior and posterior semicircular canals form are all present,

228 and fusion occurs at the correct time. However, the pillars are located closer to the dorsal

229 otic epithelium within the otic vesicle and the dorsolateral septum (DLS) that separates the

230 anterior and posterior canals does not form correctly (Fig. 1B). The mutation does not

231 appear to affect development of other organs or the size or length of the embryo significantly

232 (Fig. 1C), and homozygous mutants are adult viable. The ear phenotype appears to be

233 almost fully penetrant (23.8% of embryos showed the ear phenotype from a cross between

234 heterozygous parents; *n*=734), but there is some variability in expressivity: in a minority of

235 mutant embryos, one or both ears had a weaker phenotype, with one canal, usually the

236 posterior, unaffected and of normal size. In a few embryos, the truncations were more

237 severe (Fig. 1D, Supplementary Fig. S1).

238 To image the semicircular canal duct abnormalities in the zebrafish ear, we crossed

239 heterozygote carriers of the mutation to a transgenic line expressing GFP in the otic

240 epithelium. This line was generated by random insertion of a construct consisting of a

241 fragment of *en2a* upstream sequence and a minimal *c-fos* promoter driving expression of

242 membrane-tagged EGFP (Supplementary Fig. S2); serendipitously, some transgenic fish

243 showed GFP expression in the ear, and were isolated on this basis. Using a TAIL PCR-

244 based approach (Liu and Whittier, 1995) and Targeted Locus Amplification (TLA, Cergentis),

245 we identified two separate genomic sites of insertion of the transgene: one in the 3' region of

246 the *smad6b* locus on Chromosome 18, and a second site on Chromosome 16 in the

247 *cysteine-rich venom protein natrin-1-like* (*cvrvpn1l*) locus (see Materials and Methods and

248 Supplementary Fig. S2). The GFP expression pattern in the transgenic line, which we have

249 named *Tg(smad6b:EGFP)*, recapitulates the endogenous expression pattern of the inhibitory

250 SMAD gene *smad6b*, including strong expression in the ear; endogenous *smad6b*

251   expression is unaffected (Supplementary Fig. S2C). We do not see any GFP expression

252   that correlates to the *crvpn1l* expression pattern as assayed by in situ hybridisation

253   (Supplementary Fig. S2).

254   The *Tg(smad6b:EGFP)* embryos provide an excellent tool for imaging otic epithelia in the

255   live zebrafish embryo from 24 hpf through to adulthood (Fig. 1D, Supplementary Fig. S1 and

256   Supplementary Movie 2). Analysis of wild-type and *bmper* mutant embryos in the

257   *Tg(smad6b:EGFP)* line at 96 hours post fertilisation (hpf) using light-sheet microscopy

258   confirmed that the anterior and posterior canal ducts were truncated, forming a blind-ended

259   stump, with the anterior canal often more strongly affected. Dorsal view optical sections

260   showed that the three sensory cristae and ventral pillar developed normally, although the

261   ears of embryos with strong *bmper* phenotypes were slightly smaller at this stage (Fig. 1D,

262   Supplementary Movie 2). The space connecting the anterior and posterior canals, which will

263   later become the crus commune, was still present and of a normal height in all *bmper* mutant

264   ears; however, the dorsolateral septum (DLS), which bisects this area at the dorsal

265   boundary between the anterior and posterior canals, was wider and flatter in *bmper* mutants

266   (Fig. 1C, D).

267   **Live imaging reveals morphological and cellular changes in anterior and posterior**

268   **canal formation**

269   Imaging of the otic vesicle revealed changes in the overall shape at 55 hpf, after the anterior

270   and posterior epithelial projections have grown in to the otic lumen and fused to form pillars

271   (Fig. 1). We used 3D-rendered images of *bmper* mutant ears in the *Tg(smad6b:EGFP)* line

272   to quantify any morphometric changes in 3D. The variability in the presence and size of the

273   canal truncations made it challenging to characterise timing of onset of differences in ear

274   shape. To orientate the ear so that all measurements were comparable, key features that

275   were not affected in the mutant were used, including the endolymphatic duct (ED) and the

276   three cristae.

277   Measurements were taken in lateral views of otic vesicle height (ED to ventral crista), width

278   (anterior to posterior cristae), distance from ED to base of the anterior projection, distance

279   between the anterior pillar and the dorsal otic epithelium, and distance across the base of

280   the lateral projection. Changes were seen in *bmper* mutants with all measurements apart

281   from height (Fig. 2). The *bmper* ear was slightly wider and the height above the anterior pillar

282   was significantly reduced, as could be seen in the DIC images where shape of the top of the

283   ear, normally domed, is more pointed in the *bmper* mutant (Fig. 1). Distance from the ED to

284   the anterior projection was also reduced (either due to reduced height of the *bmper* otic

285   vesicle, or to abnormal positioning of the anterior projection). One change that was only

9

286 apparent from the fluorescent images is the width of the lateral projection. In wild-type

287 embryos, the lateral projection grows into the otic lumen as a single evagination, bifurcating

288 to form the anterior and posterior bulges that meet and fuse with the anterior and posterior

289 projections, respectively. In *bmper* mutants, the lateral projection grows into the lumen, but

290 the base of the projection is wider, and the anterior and posterior bulges are more widely

291 separated. This combination of the wider lateral projection and the reduced gap above the

292 anterior pillar means that the hub of the canal forms closer to the edge of the otic vesicle,

293 and is a possible cause of the canal truncations.

294 The dorsolateral septum (DLS) dividing the anterior and posterior canal ducts at the dorsal

295 part of the ear is also abnormal in *bmper* mutants. Analysis of the region dorsal to the lateral

296 projection revealed changes in cell shape and organisation (Fig. 2). In wild-type embryos at

297 55 hpf, the cells above the lateral projection begin to elongate in the dorsoventral axis, and

298 align to form the DLS. In *bmper* mutants, cells fail to align in an organised way. Cell shape

299 changes were also found at the sites of the canal truncations. Here, cells appeared more

300 tightly packed and were either smaller and rounded or elongated toward the truncation point

301 in *bmper* mutants, whereas in the wild-type, cells on the outer wall of the canal have a

302 squamous morphology (Fig. 2). We also noted that in *bmper* mutants with a weaker

303 phenotype, where the canal duct had not truncated, a band of elongated cells was still

304 present at a region that is the likely site where a truncation would have occurred. This

305 suggests that changes in cell shape observed in *bmper* mutants do not always result in the

306 truncation of the canal.

307 **Identification of mutations that disrupt the *bmper* gene**

308 To identify the genetic lesion underlying the mutant phenotype, we used RNAmapper (Miller

309 et al., 2013) to search for candidate causative SNPs in the mutant exome. We found that

310 the mutation maps to chromosome 16 roughly at position 10,000,000, or between 1,500,000

311 and 15,000,000 (Fig. 3A, Supplementary Fig. S3). Within this interval, we detected the gain

312 of a STOP codon with 8-fold coverage at position 9261799 (tGg>tAg, or W>*) in the *BMP-*

313 *binding endothelial regulator* (*bmper*) gene (ENSDARG00000101980 – GRCz11), formerly

314 known as *crossveinless 2* (*cv2, cvl2*; *bmper* is the orthologue of *Drosophila crossveinless 2*

315 (*cv-2*)). Sequencing of genomic DNA prepared from individual embryos (*n*=20) from a cross

316 between heterozygous parents confirmed linkage of the G>A SNP with the ear phenotype

317 (Fig. 3B). The Sanger Centre has reported the identical mutation in their collection

318 (*bmper*[sa108]), which was derived from the same round of mutagenesis (E. Busch-Nentwich,

319 personal communication), lending further support to our sequencing results. Presumably,

10

320 the *bmper^sa108* and *otx1b^sa96* lines are descendants of the same mutagenised male; we

321 therefore adopted the designation *bmper^sa108* for the mutation.

322 The Bmper protein sequence predicts a secreted glycoprotein containing five conserved

323 cysteine-rich von Willebrand factor (vWF) type C domains. The STOP codon in the

324 *bmper^sa108* allele falls at amino acid position 549, within the vWFD domain. Interestingly, this

325 is very close to the position of disease-causing mutations in the human gene (Fig.

326 3C)(Kuchinskaya et al., 2016). The mutation thus predicts a truncated protein in which the

327 vWFC domains remain intact, but the uncharacterised cysteine-rich and conserved Trypsin

328 Inhibitor domains towards the C terminus are lost (Fig. 3C). Importantly, the STOP codon is

329 downstream of the predicted cleavage site required for conversion of Bmper from an anti- to

330 a pro-BMP factor (Rentzsch et al., 2006), suggesting that the predicted protein product could

331 retain some pro-BMP activity. We therefore compared *bmper^sa108* to two further alleles,

332 *bmper^del2* and *bmper^del5*, generated in one of our laboratories (MCM) by TALEN

333 mutagenesis. These alleles have 2- and 5- base pair deletions, respectively; both result in a

334 frame-shift leading to a STOP codon at amino acid position 223, between the third and

335 fourth vWFC domains (Fig. 3C). Although the STOP codon in these *bmper^del2* and *bmper^del5*

336 alleles is upstream of the predicted cleavage site, the ear phenotype is indistinguishable

337 from that in *bmper^sa108* mutants, and the mutations, like *bmper^sa108*, are also adult viable

338 (Supplementary Fig. S3).

339 **Expression of *bmper* mRNA in the developing zebrafish ear**

340 Previous studies have described the expression pattern of the *bmper* transcript in the wild-

341 type zebrafish embryo (Esterberg and Fritz, 2009; Kudoh et al., 2001; Kwon and Riley, 2009;

342 Moser et al., 2007; Rentzsch et al., 2006). The otic vesicle is a major site of expression,

343 which has not previously been studied in detail (Fig. 3D, Supplementary Fig S3). In wild-

344 type embryos, expression is present in the posterior otic epithelium at the 12-somite stage

345 (12S), later spreading anteriorly across the dorsal otic epithelium. At 24-30 hpf, expression

346 is present throughout dorsal region, with higher expression in the anterior and posterior

347 poles at 24 hpf, while *bmper* expression is absent in ventral otic epithelium. During

348 outgrowth of the epithelial projections that form the semicircular canal system, *bmper* is

349 expressed in the epithelium that forms the outer walls of the canal ducts, and at lower levels

350 in the projections and bulges that fuse to form the pillars (the 'hubs' of each semicircular

351 canal). By 2 dpf, expression appears more ventrally at the margins of the sensory cristae,

352 and by 3 dpf, weak expression persists throughout the semicircular canal system, together

353 with the support cell layer of the sensory maculae and cristae (Supplementary Fig. S3).

354

355 In *bmper^sa108* mutants at 3 dpf, RNAmapper analysis detected a small (less than two-fold)

356 but significant (*p*=0.002) reduction in expression of one of two *bmper* isoforms. As RNA for

357 this analysis was taken at a stage when the semicircular canal duct truncation was already

358 apparent, we verified this reduction in *bmper* mRNA levels in *bmper^sa108* mutants at earlier

359 developmental stages by in situ hybridisation (Fig. 3D). The observed systemic reduction in

360 *bmper* transcript levels could be due to nonsense-mediated mRNA decay of the mutant

361 transcript, or could reflect a reduction in BMP signalling activity, as *bmper* is a known

362 transcriptional target of BMP signalling (Reichert et al., 2013; Rentzsch et al., 2006).

363 In the mouse, Bmper has been proposed as a candidate target gene for Tbx1, although

364 Tbx1 binding sites in the murine *Bmper* gene were not reported to be conserved with the

365 zebrafish (Castellanos et al., 2014). We examined the expression of *bmper* in *tbx1^-/-* mutant

366 embryos, which have a severe ear phenotype, with absent or vestigial epithelial projections

367 (Radosevic et al., 2011; Whitfield et al., 1996), but did not see major differences in the levels

368 of *bmper* expression (Supplementary Fig. S3E). Expression of *bmper* that normally marks

369 the cristae in the ventral part of the ear was lost, but this is to be expected, as cristae do not

370 develop in the *tbx1^-/-* mutant ear. *bmper* expression levels were also unaffected in *sox10^-/-*

371 mutant embryos (Supplementary Fig. S3).

Expression of otic markers in *bmper^sa108* mutants reveals specific defects in dorsal

otic epithelium

374 To understand the basis of the otic phenotype in *bmper* mutants further, we examined

375 expression of other otic markers in the ear of *bmper^sa108* mutant embryos over a range of

376 developmental stages using in situ hybridisation. We first focussed on orthologues of *Dlx5*

377 and *Hmx3*, known to be targets of BMP signalling in the developing chick ear (Ohta et al.,

378 2016). In zebrafish, *dlx5a* and *hmx3a* expression domains overlap with that of *bmper* in the

379 dorsal otic vesicle from 24 hpf to 48 hpf (Fig. 4). We found robust changes in the expression

380 pattern of *dlx5a*, which was prematurely lost in dorsal otic epithelium from 30-48 hpf, initially

381 at the anterior and posterior poles, but retained in the cristae and ED (Fig. 4). Expression of

382 *dlx5a* at earlier (27 hpf) and later (72 hpf) stages did not show any changes in level or spatial

383 extent in *bmper^sa108* mutant embryos (Fig. 4). The wild-type otic expression pattern of

384 zebrafish *hmx3a* is complex at 40 hpf, with discrete bands of expression in the anterodorsal

385 and posterodorsal domains, but lacking in the dorsal region where the ED will form and a in

386 small anterior gap (Fig. 4) (Hartwell et al., 2019). Quantification of the spatial extent of

387 *hmx3a* domains of expression revealed subtle and transient differences in the *bmper* mutant

388 ear, although levels appeared unaltered. The anterodorsal band of *hmx3a* expression was

389 reduced in *bmper^sa108* mutants, and the dorsal gap in expression, which includes part of the

12

390   same region that lacks *dlx5a* expression, was expanded (Fig 4). By 72 hpf, however, the

391   *hmx3a* otic expression pattern in *bmper*^{sa108} mutant embryos was indistinguishable from the

392   wild type (Fig. 4).

393   Despite the obvious structural defect in the ear, additional markers that we tested were

394   expressed normally, including those for the otic placode (*sox10, pax2a*), patterning at the

395   early otic vesicle stage (*aldh1a3, hmx2a, otx1b*), sensory patch development (*pax2a*) and

396   otic neurogenesis (*neurod*) (Supplementary Fig. S4). Of note, the normal expression

397   domain of *otx1b* in ventral otic epithelium correlates with the normal formation of the ventral

398   pillar and lateral (horizontal) semicircular canal duct (Fig. 1). Other markers for dorsal otic

399   epithelium (*dlx3a, gbx2, dacha, lmx1ba, fn1a*) and the endolymphatic duct (*foxi1*) were

400   expressed normally in *bmper* mutants (Supplementary Fig. S4). At 30 hpf, *bmper* is strongly

401   expressed at the anterior and posterior poles of the otic vesicle; however, three of the genes

402   that are co-expressed at this time, *fn1a*, *prdm1* and the proliferation marker *pcna*, all had

403   unaltered patterns of expression in *bmper*^{sa108} mutant embryos (Supplementary Fig. S4).

404   Similarly, we analysed other markers of semicircular canal morphogenesis required for the

405   formation of the epithelial projections that form pillars of tissue that will become the internal

406   walls of the semicircular canal ducts (*adgrg6, vcana, ugdh, lmo4b, lmx1bb*). All these

407   markers were expressed at normal levels in mutant embryos (Supplementary Fig. S4).

408   **Effect of the *bmper*^{sa108} mutation on BMP signalling in the developing ear**

409   To examine the effect of the *bmper* mutation on BMP signalling, we examined the

410   expression of genes coding for BMP signalling pathway components in and around the

411   developing ear. We compared expression of *bmp2b, bmp4, bmp6, bmp7b, smad6a,*

412   *smad6b* and *chordin* in wild-type and *bmper* mutant otic vesicles at 30 hpf, a stage just prior

413   to the first morphological changes seen in *bmper* mutant embryos, and at 48 hpf, when

414   subtle changes in otic morphology become evident. However, we did not detect any

415   significant differences in expression of BMP pathway genes in *bmper* mutant ears (Fig. 5A).

416   At 30 hpf, expression of *bmp2b* and *bmp4* is strong in the anterior posterior poles of the otic

417   vesicle, overlapping with expression of *bmper*, whereas *bmp6* is only expressed dorsally.

418   *bmp7b* is expressed in the periotic mesenchyme in two dorsal areas at the anterior and

419   posterior of the vesicle adjacent to the region of *dlx5*a expression that is absent in *bmper*

420   mutants (Fig. 5A). By 48hpf, *bmp2b* and *bmp4* expression expands dorsally; both still

421   overlap with *bmper* but in different regions. Expression of *bmp4* overlaps with that of *gbx2*

422   at the site of the developing ED, and *bmp2b* has weak expression in the anterior dorsal

423   region, where *dlx5a* expression is lost. Both *bmp2b* and *dlx5a* are also strongly expressed

424   in the cristae. *bmp6* and *bmp7b* become strongly expressed in the epithelial projections at

425   48 hpf. Two genes coding for negative regulators of BMP signalling are also expressed at

426   these stages. We observed a transient focus of expression of *chordin* in the dorsal periotic

427   mesenchyme, overlapping with the expression of *bmp7b* at 30 hpf. Subtle increases in the

428   area of *bmp7b* expression domain in the periotic mesenchyme were noted in *bmper*

429   mutants. The inhibitory SMAD gene *smad6b* is strongly expressed throughout the otic

430   vesicle (Supplementary Fig. S2). However, we found no change in levels of GFP

431   fluorescence in *bmper* mutant ears, or in the strength of the *bmper* otic phenotype, in the

432   *Tg(smad6b:EGFP)* background.

433   To determine if BMP signalling activity was affected in the *bmper* mutant ear, we analysed

434   levels of P-Smad5 in the otic vesicle at 32 hpf and 48 hpf using quantitative

435   immunofluorescence. The strongest activity at 32 hpf was seen at the anterior and posterior

436   poles of the otic vesicle, where *bmp2b* and *bmp4* are also expressed. In *bmper^{del2}* mutant

437   embryos, P-Smad5 levels were significantly decreased compared with heterozygous

438   siblings. By 48 hpf, the strongest BMP activity was detected in the two sensory maculae,

439   with low levels of P-Smad5 elsewhere in the otic epithelium. By comparing relative levels of

440   P-Smad5, a reduction in BMP pathway activity was detected in non-sensory dorsal otic

441   epithelium of *bmper^{del2}* mutant embryos (Fig. 5K–P).

442   To confirm this result and measure BMP pathway activity in live embryos, we crossed

443   *bmper^{sa108+/-}* fish to the BMP reporter line *Tg(BMPRE:mRFP)* (Reichert et al., 2013). From

444   24 hpf, mRFP expression was predominantly in the anterior and posterior poles of the otic

445   vesicle and also in the lateral region where the lateral projection will form. At 24 hpf, no

446   difference was detected between wild-type and *bmper* mutant ears; however, the mRFP is

447   not destabilised and may persist from earlier expression. A clear difference between wild-

448   type siblings and *bmper* mutants was seen by 48 hpf: in wild-type embryos, mosaic

449   expression of mRFP was observed in dorsal otic epithelium, which was absent in the *bmper*

450   mutant ear. At 72 hpf, the semicircular canal duct truncations were already evident in the

451   *bmper* mutant ear; mRFP expression was absent in canal wall epithelium in mutant

452   embryos, but was strongly expressed in the cristae in both the wild-type and *bmper* mutant

453   ear (Fig. 5Q–T). Taken together, the reduction in P-Smad5 staining and fluorescence levels

454   of the BMP transgenic reporter suggest that Bmper is normally required to promote BMP

455   signalling in in non-sensory otic epithelium, but does not appear to be required for BMP

456   signalling in otic sensory tissue. We also noted a slight increase in mRFP fluorescence

457   levels surrounding the otic vesicle at both stages in *bmper* mutants (Fig. 5Q–T). This might

458   indicate that Bmper is required to repress BMP pathway activity in periotic mesenchyme.

There are no substantial neural crest, cardiovascular or pronephric abnormalities in *bmper* mutant embryos

Over-expression studies in the chick and morpholino-based knockdown in the zebrafish have implicated Bmper in promoting development of the neural crest (Coles et al., 2004; Reichert et al., 2013). To test whether neural crest fates are affected in the *bmper*[sa108] mutant, we examined development of neural crest derivatives (craniofacial cartilages, pigment cells and Schwann cells). Although the cartilage stains were more variable in mutants, all elements of the craniofacial skeleton were present (Fig. 6). Pigmentation of larval and adult fish appeared largely normal; all three pigment cell types (melanocytes, xanthophores and iridophores) were present, and the stripe pattern was normal (Fig. 6). In addition, expression of the neural crest markers *foxd3* and *sox10* was present and apparently unaffected in *bmper*[sa108] mutant embryos, as was expression of *myelin basic protein* mRNA marking the presence of neural-crest-derived Schwann cells (Fig. 6).

Previous studies employing morpholino-mediated knockdown of *bmper* have reported defects in the tail vasculature, including defects in the intersegmental vessels (ISVs), dorsal longitudinal anastomotic vessel (DLAV) and caudal vein plexus (CVP) (Dyer et al., 2015; Heinke et al., 2013). To check whether there were any similar abnormalities in *bmper*[sa108] mutants, we examined the expression of *ve-cadherin* mRNA, a marker of vascular endothelium. We did not find similar defects or any consistent changes in vasculature patterning in developing *bmper* mutants (Fig. 5). Early patterning of the pronephros was assessed by *pax2a* expression, also unchanged in *bmper* mutants. Taken together, our analyses indicate that there are no substantial defects in the development of neural crest or cardiovascular derivatives in zygotic *bmper* embryos in the zebrafish, although we cannot rule out subtle defects in these or other tissues.

Previous studies have described moderate dorsalisation phenotypes following morpholino-mediated knockdown of *bmper* in the zebrafish, indicating an early requirement in promoting BMP signalling to establish ventral identity in the early embryo (Moser et al., 2007; Rentzsch et al., 2006). We have not found any evidence for this in the zygotic *bmper* mutants; embryonic axial patterning appeared normal in all embryos.

Anatomy of the ear in adult *bmper*[sa108] mutants

The zebrafish zygotic *bmper* mutant alleles described here are adult viable and fertile. To examine the effect of the embryonic otic patterning defects on post-embryonic ear development we used lightsheet microscopy to analyse ear morphology at 21 dpf. At this stage in both wild-type and *bmper* mutant ears, the semicircular canal ducts have begun to elongate and the truncated canal ducts in the mutant have separated from the dorsal tissue.

494   In some specimens, a section of the canal duct remains attached to the crus commune,

495   which is clearly visible. In the *bmper* mutant there can be a significant difference in the

496   length of the anterior and posterior canals. The 90° angle between the anterior and posterior

497   canals can be seen in the wild type and in *bmper* mutant ears. In all juvenile and adult ears

498   that we examined, the lateral (horizontal) canal was present, complete, and relatively normal

499   in morphology. All three ampullae, each containing a crista, were present.

500   To study the adult ear anatomy, we dissected ears from fixed adult homozygous *bmper^{sa108}*

501   mutant fish. Truncations of the anterior and posterior semicircular canal ducts persist into

502   adulthood (Fig. 7). Some ears displayed severe truncations, where the canal duct was no

503   more than a small bud attached to the ampulla (Fig. 7A-C), but in others the canal ducts

504   extended some distance from the ampulla before ending blindly (Fig. 7E). The

505   *Tg*(*smad6b:EGFP*) transgene is still expressed in adult ear tissue, enabling the cellular and

506   structural detail of the adult canals to be imaged using this fluorescent marker. The

507   truncated semicircular canal ducts have a normal diameter and curve in the correct

508   orientation compared to the wild type.

509

16

Discussion

Zygotic Bmper function is required for correct morphogenesis of the anterior and posterior semicircular canal ducts in the developing ear

We have characterised two new mutant alleles of the BMP regulator gene *bmper*, both of which cause dorsal truncations of the anterior and posterior semicircular canals in the zebrafish inner ear. The nature and specificity of the ear phenotype were unexpected; to our knowledge, otic defects have not been described in murine *Bmper* mutants, and previous studies based on morpholino-mediated knockdown and mRNA mis-expression in the zebrafish have inferred roles for Bmper in embryonic axial patterning, placodal and neural crest specification and endothelial development, phenotypes that are not recapitulated in the zygotic mutants. However, the otic defects we describe in the zebrafish *bmper* mutants fit well with the known conserved role of BMP signalling in the inner ear.

BMP signalling is known to play an important role in semicircular canal formation in mice, chick and zebrafish (reviewed in (Alsina and Whitfield, 2017)). Our previous work demonstrated a requirement for Bmp2b function in the development of all three semicircular canal ducts in the zebrafish ear (Hammond et al., 2009), and this requirement is conserved in mice (Hwang et al., 2019). The *bmper* mutant phenotype is more specific and less severe than that in *bmp2b* mutants, only affecting the anterior and posterior ducts, and resulting in dorsal truncations of these structures in the adult ear. In amniote ears, the anterior and posterior canal ducts, together with the crus commune, develop from a dorsolateral pouch, whereas the horizontal (lateral) canal develops from a lateral pouch (reviewed in (Alsina and Whitfield, 2017)). Thinning of the dorsolateral pouch in the chick is dependent on BMP signalling, and correlates with pSMAD activity (Ohta et al., 2010). Pouches are not so evident in the developing zebrafish ear, but the *bmper* mutant phenotype demonstrates that the anterior and posterior canals share genetic requirements that are separate from those for the lateral (horizontal) canal, as in amniotes. We therefore propose that a region of the zebrafish otic vesicle exists that is the equivalent of the dorsolateral canal pouch in amniote ears, and is dependent on the promotion of BMP signalling by Bmper for its normal morphogenesis.

The lateral (horizontal) canal duct develops relatively normally and is complete in the adult *bmper* mutant ear. This reflects the normal expression of *otx1b* at otic vesicle stages in *bmper* mutants, and normal appearance of the ventral pillar. Otx1 function is known to be required for formation of the lateral canal in both zebrafish and mammals (reviewed in (Alsina and Whitfield, 2017)). The endolymphatic duct, which is a dorsal otic structure, also appears to be unaffected in the *bmper* mutant ear. Interestingly, endolymphatic duct

545 outgrowth was also unaffected by overexpression of the BMP inhibitor gene Noggin in the

546 chick (Ohta et al., 2010). Taken together, our results suggest that patterning of the otic

547 dorsoventral axis is unaffected in *bmper* mutants, but reveal a specific requirement for

548 Bmper in the morphogenetic events that convert dorsolateral otic epithelium into the anterior

549 and posterior canal ducts.

550 It is interesting that all three ampullae and cristae apparently form normally in the *bmper*

551 mutant ear. Expression of BMP genes in cristae is highly conserved across vertebrates

552 (Hemmati-Brivanlou and Thomsen, 1995; Morsli et al., 1998; Mowbray et al., 2001; Wu and

553 Oh, 1996), and crista development is dependent on Bmp4 function in the mouse (Chang et

554 al., 2008). Moreover, mis-expression of inhibitors of BMP signalling (Smad6, Noggin)

555 resulted in the down-regulation of expression of crista-associated genes in the chick (Chang

556 et al., 2008). However, we found that ampullae and cristae formed in the absence of Bmp2b

557 function in the zebrafish (Hammond et al., 2009), as in the *bmper* mutants. The *bmper* gene

558 has an expression domain that overlaps with that of *bmp2b* in the zebrafish ear (Mowbray et

559 al., 2001). These data may indicate that Bmper acts to modify Bmp2b-dependent signalling

560 in the ear. Additionally, other BMPs known to interact with Bmper are co-expressed with

561 *bmper* in different domains of the ear and may contribute to the defect in canal formation.

562 These domains include the area of expression of *bmp4* and *bmp2b* at the anterior and

563 posterior poles of the otic vesicle at 30 hpf, the expression of *bmp6* and *bmp7b* in the

564 epithelial projections, and the expression of *bmp7b* and *chordin* in periotic mesenchyme

565 adjacent to the site where the canal truncations form.

566 **Transcriptional targets of *bmper* expression in the zebrafish ear**

567 Our results identify *dlx5a* as a likely transcriptional target of canonical BMP/SMAD signalling

568 in the zebrafish ear, potentiated by Bmper. The *dlx5a* gene is expressed in a similar pattern

569 to both *bmp2b* and *bmper* in the dorsal otic vesicle in zebrafish at the 20-25 somite stage

570 (Solomon et al., 2003; Thisse and Thisse, 2004), and *dlx5a* expression is lost in dorsal otic

571 epithelium (excepting the endolymphatic duct) in the *bmper*^{sa108} mutant. A reciprocal

572 relationship is found in the mouse, where several lines of evidence identify *Bmper* as a likely

573 direct transcriptional target of Dlx5 in the otocyst (Sajan et al., 2011); murine *Bmper*

574 expression is also dependent on Dlx5/6 in the branchial arches (Jeong et al., 2008).

575 *Dlx* genes have a known function in semicircular canal development in the mouse: canal

576 ducts fail to form correctly in the murine *Dlx5* mutant ear (Acampora et al., 1999; Merlo et al.,

577 2002), while in the double *Dlx5/6* mouse mutant ear, there is a loss of all dorsal derivatives,

578 including the semicircular canals, correlating with a loss of otic *Gbx2*, *Bmp4* and *Otx1*

579 expression at early stages (Robledo and Lufkin, 2006). It is likely that these changes are

18

580   mediated, at least in part, through regulation of BMP signalling, as manipulation of BMP

581   signalling results in similar phenotypes. Conditional disruption of Bmp4 in the mouse ear

582   results in down-regulation of *Dlx5* expression, although *Dlx5* expression remains in the ED

583   (Chang et al., 2008), similar to the pattern we see in zebrafish *bmper* mutants. Dorsomedial

584   Dlx5 and Gbx2 expression is also responsive to Wnt signalling (Lin et al., 2005; Merlo et al.,

585   2002).

586   Non-canonical BMP/PKA signalling also regulates the expression of *Hmx3* in the chick ear

587   (Ohta et al., 2016). Our data revealed only subtle changes in the spatial extent of otic

588   *hmx3a* expression in the *bmper* mutant ear, and *hmx3a* expression persisted in the

589   dorsolateral regions where *dlx5a* expression is lost in *bmper* mutants. Thus, *hmx3a* does

590   not appear to be a major transcriptional target of *bmper*-mediated BMP signalling in the

591   zebrafish ear. Otic expression of *hmx3a* is instead known to be regulated by Fgf and

592   Hedgehog signalling in the zebrafish, and is required for normal otic anterior patterning

593   (Hartwell et al., 2019).

594   **Structure and function of the zebrafish Bmper protein**

595   Bmper, together with its *Drosophila* orthologue Crossveinless-2 (Cv-2), is a known regulator

596   of BMP signalling with both pro-BMP and anti-BMP activity in different contexts (Conley et

597   al., 2000; Rentzsch et al., 2006; Serpe et al., 2008; Zhang et al., 2010). In the fly, secreted

598   Cv-2 protein interacts with heparan sulphate proteoglycans on the cell surface, where it fine-

599   tunes BMP signalling in a concentration-dependent manner (O'Connor et al., 2006; Serpe et

600   al., 2008). In the fish, morpholino-mediated knockdown of *bmper* has been reported to

601   cause moderate embryo dorsalisation, indicating that the protein normally functions to

602   promote BMP activity during patterning of the embryonic dorsoventral axis (Moser et al.,

603   2007; Rentzsch et al., 2006; Zhang et al., 2010). However, injection of full-length *bmper*

604   mRNA gave rise to a full spectrum of dorsalised and ventralised phenotypes, suggesting

605   both pro- and anti-BMP activity (Rentzsch et al., 2006; Zhang et al., 2010). The proposed

606   explanation for this apparently contradictory finding is that cleavage of Bmper converts it

607   from an anti- to a pro-BMP factor: injection of mRNA coding for an uncleavable protein has

608   strong dorsalising activity, while that coding for the cleaved N-terminal fragment alone

609   (amino acids 1-355) has strong ventralising activity (Rentzsch et al., 2006). Zhang and

610   colleagues report that the anti-BMP function is effected by binding to BMP, while the pro-

611   BMP function is mediated through binding to Chordin (Zhang et al., 2010). The different

612   cleaved versions are also proposed to have similar affinities to BMPs but different affinities

613   to the extracellular matrix which is thought to interact with Bmper through the C terminus

614   (Rentzsch et al., 2006). The data we have presented here for the zebrafish *bmper* mutant

19

615 phenotype, including the comparison to known BMP loss-of-function otic phenotypes and the

616 reduction in P-Smad5 and BRE activity in otic tissue, all indicate a pro-BMP function for

617 Bmper in the zebrafish ear.

618 The Bmper protein has structural similarity with the BMP inhibitor protein Chordin (Rentzsch

619 et al., 2006), and some conservation with the larger glycoproteins alpha-Tectorin and

620 Otogelin, which have roles in otolith tethering in the developing zebrafish ear (Stooke-

621 Vaughan et al., 2015). However, otolith formation and tethering appear normal in the *bmper*

622 mutant ear (this work), and semicircular canals form normally in *tecta* and *otog* mutants

623 (Stooke-Vaughan et al., 2015), so the functions of these structurally related glycoproteins do

624 not appear to overlap in the zebrafish ear.

625 It is likely that the discrepancies between the mutant phenotype described here and the

626 much more severe effects on embryonic patterning due to morpholino knockdown (Moser et

627 al., 2007; Rentzsch et al., 2006; Zhang et al., 2010) are partly due to genetic compensation

628 via transcriptional adaptation (El-Brolosy et al., 2019; Sztal and Stainier, 2020). However, it

629 is also possible that the *bmper^sa108^* allele is hypomorphic, and that the mutant protein, if

630 produced, retains some function. The STOP codon is downstream of the cleavage site after

631 amino acid 353, and so the mutant protein might be expected to undergo cleavage and

632 generate an N-terminal fragment with pro-BMP (ventralising) function. The ear phenotype,

633 however, is indistinguishable between the *bmper^sa108^* and *bmper^del2^* alleles, and thus both

634 may represent complete loss of function for otic morphogenesis. Bmper has been shown to

635 bind Bmp2/7 through vWFC1 (Zhang et al., 2007), which remains intact in the predicted

636 mutant proteins, and so it is possible that some anti-BMP function is retained in the mutants,

637 and is perhaps active in other tissues.

638 **Zebrafish Bmper does not appear to function in establishment of the preplacodal**

639 **region, otic placode or neural crest**

640 Competence to form the pre-placodal region (PPR) that gives rise to the otic placode relies

641 on active BMP signalling at late blastula stages, followed by a specification step involving

642 attenuation of BMP signalling in the late gastrula (Bhat et al., 2013) (and references within).

643 Previous studies using morpholino-based knockdown have suggested that Bmper acts as a

644 BMP antagonist in generation of the PPR. Kwon and Riley proposed that *bmper* is one of a

645 number of BMP antagonist genes expressed in cephalic paraxial mesendoderm that

646 together contribute positively to otic induction from the PPR, although they found 'little or no

647 effect' on development of the ear following morpholino-mediated knockdown of *bmper* alone

648 (Kwon and Riley, 2009). On the other hand, Esterberg and Fritz reported expression of

649 *bmper* in the PPR (ectoderm) itself, and that morpholino-mediated knockdown of *bmper*

650 resulted in a circular otic vesicle with no otoliths, similar to that of *dlx3b/4b* morpholino

651 knockdown (Esterberg and Fritz, 2009). Using morpholino-based knockdown and mRNA

652 mis-expression experiments, these authors also suggested a role for Bmper in attenuating

653 BMP activity to establish the PPR and to confer competence to respond to FGF signalling

654 (Esterberg and Fritz, 2009). However, a subsequent study has challenged this

655 interpretation; Reichert and colleagues have shown that *bmper* is expressed in the zones of

656 higher BMP activity either side of the PPR, and propose that it acts locally to promote BMP

657 activity and expression of neural crest markers. Their study identifies the BMP antagonist

658 *bambib* as responsible for attenuation of BMP signalling in the PPR (Reichert et al., 2013).

659 In zygotic homozygous *bmper* mutants, we see very little effect on PPR specification, otic

660 placode induction, early otic vesicle shape, otolith formation or neural crest specification.

661 Notably, we do not find any reduction in expression of the otic placode marker *pax2a*, or of

662 the neural crest markers *foxd3* and *sox10*, contrary to previous reports of down-regulation of

663 these genes following morpholino-based knockdown of *bmper* (Esterberg and Fritz, 2009;

664 Reichert et al., 2013). If *bmper* conferred competence to respond to FGF signalling during

665 otic induction and patterning, we might expect the mutant otic phenotype to resemble that of

666 embryos with compromised FGF signalling (Hammond and Whitfield, 2011; Hartwell et al.,

667 2019; Léger and Brand, 2002; Maier and Whitfield, 2014)—but this is not the case. Our

668 results, therefore, do not support a role for Bmper in PPR specification, otic placode

669 induction or neural crest specification.

670 In the mouse, a differential RNAseq study of dissected otocysts identified *Bmper* as a

671 significantly upregulated transcript following conditional ablation of *FGFR2b* over different

672 time windows between E9 and E12; ventral expansion of the *Bmper* otic expression domain

673 was validated by in situ hybridisation (Urness et al., 2018). These results implicate

674 signalling via the FGFR2b ligands FGF3 and FGF10 in limiting *Bmper* expression to dorsal

675 otic epithelium in the mouse.

Expression and roles in other tissues, and comparison with mammalian *Bmper*

676

677 **mutant phenotypes**

678 It is puzzling that the phenotype in the zebrafish *bmper* mutants appears to be so restricted

679 to the ear. The zebrafish *bmper* gene itself is expressed in many other tissues, including

680 paraxial mesendoderm, neural plate border, epiphysis, lens, cloaca, and elements of the

681 developing craniofacial skeleton and vasculature (Clément et al., 2008; Esser et al., 2018;

682 Esterberg and Fritz, 2009; Kessels et al., 2014; Kudoh et al., 2001; Kwon and Riley, 2009; Li

683 et al., 2009; Lockhart-Cairns et al., 2019; Moser et al., 2007; Reichert et al., 2013; Rentzsch

684 et al., 2006). It was not our intention here to provide a comprehensive analysis of tissues

685 other than the ear, and it is quite possible that additional defects are present. However, the

686 overall phenotype is clearly less severe in fish than in mammals (see below). This could

687 reflect sub-functionalisation with a paralogous gene in the fish, but the *bmper* gene appears

688 to be unique in the zebrafish genome; there is no predicted gene duplicate. Another

689 possible interpretation is that the C-terminal truncations predicted for the *bmper^sa108^* and

690 *bmper^del2^* alleles remove a portion of the protein that is critical for function in the ear, but not

691 in other organ systems. It seems unlikely, however, that the severe truncation in the

692 *bmper^del2^* allele is able to retain significant protein function.

693 Mutations in the murine *Bmper* gene cause cardiovascular, skeletal and renal phenotypes,

694 all indicative of a pro-BMP function for the wild-type protein (Dyer et al., 2014; Ikeya et al.,

695 2006; Ikeya et al., 2010). To our knowledge, the inner ear phenotype has not been

696 characterised in the mouse, although *Bmper* is expressed in the murine otic vesicle

697 (Coffinier et al., 2002; Ikeya et al., 2006; Urness et al., 2018). In humans, recessive

698 mutations in *BMPER* are causative for a family of rare skeletal dysplasias including

699 diaphanospondylodysostosis (DSD), symptoms of which include delayed or absent vertebral

700 ossification, missing ribs and craniofacial and renal anomalies (Ben-Neriah et al., 2011;

701 Funari et al., 2010; Gonzales et al., 2005; Greenbaum et al., 2019; Hofstaetter et al., 2018;

702 Kuchinskaya et al., 2016; Legare et al., 2017; Zong et al., 2015) (OMIM 608022). The most

703 severe cases are perinatal lethal due to respiratory insufficiency; hearing loss was reported

704 in two patients surviving beyond infancy (Kuchinskaya et al., 2016; Scottoline et al., 2012).

705 Four siblings presenting with severe congenital scoliosis, but a lack of renal anomalies, were

706 shown to be transheterozygous for mutations in *BMPER* (Zong et al., 2015). Notably, two of

707 the human mutations described predict a similar protein truncation to *bmper^sa108^*, with a loss

708 of the C-terminal cysteine-rich and trypsin inhibitor domains (Kuchinskaya et al., 2016; Zong

709 et al., 2015) (Fig. 3C). More recent studies have identified a role for BMPER in insulin

710 resistance and obesity (Mao et al., 2021; Pérez et al., 2021), which could also be tested for

711 in the adult viable zebrafish mutants. No study has been made of any vestibular anomalies

712 in the human DSD patients, to our knowledge. The zebrafish mutants will be useful in

713 prompting such studies, and may help to improve our understanding of the pathology of

714 these rare disorders.

Acknowledgements

720   expert fish husbandry, and thank the Sanger Institute Zebrafish Mutation Resource for

721   providing the *otx1b^{sa96}* mutant allele, which led to the discovery of *bmper^{sa108}* in the

722   background in the Whitfield lab. The Mullins lab obtained the *bmper^{sa108}* line directly from

723   the Sanger collection.

733

References

Acampora, D., Merlo, G. R., Paleari, L., Zerega, B., Postiglione, M. P., Mantero, S., Bober, E., Barbieri, O., Simeone, A. and Levi, G. (1999). Craniofacial, vestibular and bone defects in mice lacking the Distal-less-related gene Dlx5. *Development* **126**, 3795–3809.

Aleström, P., D'Angelo, L., Midtlyng, P. J., Schorderet, D. F., Schulte-Merker, S., Sohm, F. and Warner, S. (2020). Zebrafish: Housing and husbandry recommendations. *Lab. Anim.* **54**, 213–224.

Alsina, B. and Whitfield, T. T. (2017). Sculpting the labyrinth: Morphogenesis of the developing inner ear. *Semin. Cell Dev. Biol.* **65**, 47–59.

Baxendale, S. and Whitfield, T. T. (2016). Methods to study the development, anatomy, and function of the zebrafish inner ear across the life course. In *Methods in Cell Biology*, pp. 165–209.

Baxendale, S., Chen, C.-K. C. K., Tang, H., Davison, C., Hateren, L. V. L. Van, Croning, M. D. R. M. D. R., Humphray, S. J. S. J., Hubbard, S. J. S. J. and Ingham, P. W. P. W. (2009). Expression screening and annotation of a zebrafish myoblast cDNA library. *Gene Expr. Patterns* **9**, 73–82.

Ben-Neriah, Z., Michaelson-Cohen, R., Inbar-Feigenberg, M., Nadjari, M., Zeligson, S., Shaag, A., Zenvirt, S., Elpeleg, O. and Levy-Lahad, E. (2011). A deleterious founder mutation in the BMPER gene causes diaphanospondylodysostosis (DSD). *Am. J. Med. Genet. Part A* **155**, 2801–2806.

Bhat, N., Kwon, H. J. and Riley, B. B. (2013). A gene network that coordinates preplacodal competence and neural crest specification in zebrafish. *Dev. Biol.* **373**, 107–117.

Castellanos, R., Xie, Q., Zheng, D., Cvekl, A. and Morrow, B. E. (2014). Mammalian TBX1 Preferentially Binds and Regulates Downstream Targets Via a Tandem T-site Repeat. *PLoS One* **9**, e95151.

Chang, W., Nunes, F. D., De Jesus-Escobar, J. M., Harland, R. and Wu, D. K. (1999). Ectopic Noggin blocks sensory and nonsensory organ morphogenesis in the chicken inner ear. *Dev. Biol.* **216**, 369–381.

Chang, W., Ten Dijke, P. and Wu, D. K. (2002). BMP pathways are involved in otic capsule formation and epithelial - Mesenchymal signaling in the developing chicken inner ear. *Dev. Biol.* **251**, 380–394.

Chang, W., Brigande, J. V., Fekete, D. M. and Wu, D. K. (2004). The development of semicircular canals in the inner ear: Role of FGFs in sensory cristae. *Development* **131**, 4201–4211.

Chang, W., Lin, Z., Kulessa, H., Hebert, J., Hogan, B. L. M. and Wu, D. K. (2008). Bmp4 Is Essential for the Formation of the Vestibular Apparatus that Detects Angular Head Movements. *PLoS Genet.* **4**, e1000050.

Clément, A., Wiweger, M., von der Hardt, S., Rusch, M. A., Selleck, S. B., Chien, C.-B. and Roehl, H. H. (2008). Regulation of Zebrafish Skeletogenesis by ext2/dackel and papst1/pinscher. *PLoS Genet.* **4**, e1000136.

Coffinier, C., Ketpura, N., Tran, U., Geissert, D. and De Robertis, E. M. (2002). Mouse Crossveinless-2 is the vertebrate homolog of a Drosophila extracellular regulator of BMP signaling. *Mech. Dev.* **119**, S179–S184.

Coles, E., Christiansen, J., Economou, A., Bronner-Fraser, M. and Wilkinson, D. G. (2004). A vertebrate crossveinless 2 homologue modulates BMP activity and neural crest cell migration. *Development* **131**, 5309–5317.

781 **Collery, R. F. and Link, B. A.** (2011). Dynamic smad-mediated BMP signaling revealed
782   through transgenic zebrafish. *Dev. Dyn.* **240**, 712–22.

783 **Conley, C. A., Silburn, R., Singer, M. A., Ralston, A., Rohwer-Nutter, D., Olson, D. J.,**
784   **Gelbart, W. and Blair, S. S.** (2000). Crossveinless 2 contains cysteine-rich domains
785   and is required for high levels of BMP-like activity during the formation of the cross
786   veins in Drosophila. *Development* **127**, 3947–3959.

787 **De Vree, P. J. P., De Wit, E., Yilmaz, M., Van De Heijning, M., Klous, P., Verstegen, M. J.**
788   **A. M., Wan, Y., Teunissen, H., Krijger, P. H. L., Geeven, G., et al.** (2014). Targeted
789   sequencing by proximity ligation for comprehensive variant detection and local
790   haplotyping. *Nat. Biotechnol.* **32**, 1019–1025.

791 **Dyer, L., Wu, Y., Moser, M. and Patterson, C.** (2014). BMPER-induced BMP signaling
792   promotes coronary artery remodeling. *Dev. Biol.* **386**, 385–394.

793 **Dyer, L., Lockyer, P., Wu, Y., Saha, A., Cyr, C., Moser, M., Pi, X. and Patterson, C.**
794   (2015). BMPER Promotes Epithelial-Mesenchymal Transition in the Developing Cardiac
795   Cushions. *PLoS One* **10**, e0139209.

796 **El-Brolosy, M. A., Kontarakis, Z., Rossi, A., Kuenne, C., Günther, S., Fukuda, N., Kikhi,**
797   **K., Boezio, G. L. M., Takacs, C. M., Lai, S.-L., et al.** (2019). Genetic compensation
798   triggered by mutant mRNA degradation. *Nature* **568**, 193–197.

799 **Esser, J. S., Steiner, R. E., Deckler, M., Schmitt, H., Engert, B., Link, S., Charlet, A.,**
800   **Patterson, C., Bode, C., Zhou, Q., et al.** (2018). Extracellular bone morphogenetic
801   protein modulator BMPER and twisted gastrulation homolog 1 preserve arterial-venous
802   specification in zebrafish blood vessel development and regulate Notch signaling in
803   endothelial cells. *FEBS J.* **285**, 1419–1436.

804 **Esterberg, R. and Fritz, A.** (2009). dlx3b/4b are required for the formation of the
805   preplacodal region and otic placode through local modulation of BMP activity. *Dev. Biol.*
806   **325**, 189–199.

807 **Felber, K., Elks, P. M., Lecca, M. and Roehl, H. H.** (2015). Expression of osterix Is
808   Regulated by FGF and Wnt/β-Catenin Signalling during Osteoblast Differentiation.
809   *PLoS One* **10**, e0144982.

810 **Funari, V. A., Krakow, D., Nevarez, L., Chen, Z., Funari, T. L., Vatanavicharn, N.,**
811   **Wilcox, W. R., Rimoin, D. L., Nelson, S. F. and Cohn, D. H.** (2010). BMPER mutation
812   in Diaphanospondylodysostosis identified by ancestral autozygosity mapping and
813   targeted high-throughput sequencing. *Am. J. Hum. Genet.* **87**, 532–537.

814 **Gerlach-Bank, L. M., Cleveland, A. R. and Barald, K. F.** (2004). DAN Directs
815   Endolymphatic Sac and Duct Outgrowth in the Avian Inner Ear. *Dev. Dyn.* **229**, 219–
816   230.

817 **Gerlach, L. M., Hutson, M. R., Germiller, J. A., Nguyen-Luu, D., Victor, J. C. and Barald,**
818   **K. F.** (2000). Addition of the BMP4 antagonist, noggin, disrupts avian inner ear
819   development. *Development* **127**, 45–54.

820 **Gonzales, M., Verloes, A., Saint Frison, M. H., Perrotez, C., Bourdet, O., Encha-Razavi,**
821   **F., Joyé, N., Taillemite, J. L., Walbaum, R., Pfeiffer, R., et al.** (2005).
822   Diaphanospondylodysostosis (DSD): Confirmation of a recessive disorder with
823   abnormal vertebral ossification and nephroblastomatosis. *Am. J. Med. Genet.* **136 A**,
824   373–376.

825 **Greenbaum, L., Gilboa, Y., Raas-Rothschild, A., Barel, O., Kol, N., Reznik-Wolf, H.,**
826   **Pode-Shakked, B., Finezilber, Y., Messing, B. and Berkenstadt, M.** (2019).
827   Diaphanospondylodysostosis: Refining the prenatal diagnosis of a rare skeletal
828   disorder. *Eur. J. Med. Genet.* **62**, 167–171.

829 **Groves, A. K. and LaBonne, C.** (2014). Setting appropriate boundaries: Fate, patterning
830 and competence at the neural plate border. *Dev. Biol.* **389**, 2–12.

831 **Hammond, K. L. and Whitfield, T. T.** (2006). The developing lamprey ear closely
832 resembles the zebrafish otic vesicle: Otx1 expression can account for all major
833 patterning differences. *Development* **133**, 1347–1357.

834 **Hammond, K. L. and Whitfield, T. T.** (2011). Fgf and Hh signalling act on a symmetrical
835 pre-pattern to specify anterior and posterior identity in the zebrafish otic placode and
836 vesicle. *Development* **138**, 3977–87.

837 **Hammond, K. L., Loynes, H. E., Mowbray, C., Runke, G., Hammerschmidt, M., Mullins,
838 M. C., Hildreth, V., Chaudhry, B. and Whitfield, T. T.** (2009). A late role for bmp2b in
839 the morphogenesis of semicircular canal ducts in the zebrafish inner ear. *PLoS One* **4**,
840 e4368.

841 **Hartwell, R. D., England, S. J., Monk, N. A. M., van Hateren, N. J., Baxendale, S., Marzo,
842 M., Lewis, K. E. and Whitfield, T. T.** (2019). Anteroposterior patterning of the zebrafish
843 ear through Fgf- and Hh-dependent regulation of hmx3a expression. *PLOS Genet.* **15**,
844 e1008051.

845 **Heinke, J., Juschkat, M., Charlet, A., Mnich, L., Helbing, T., Bode, C., Patterson, C. and
846 Moser, M.** (2013). Antagonism and synergy between extracellular BMP modulators Tsg
847 and BMPER balance blood vessel formation. *J. Cell Sci.* **126**, 3082–94.

848 **Hemmati-Brivanlou, A. and Thomsen, G. H.** (1995). Ventral mesodermal patterning in
849 Xenopus embryos: Expression patterns and activities of BMP-2 and BMP-4. *Dev.
850 Genet.* **17**, 78–89.

851 **Hofstaetter, C., Courage, C., Bartholdi, D., Biskup, S. and Raio, L.** (2018). Prenatal
852 diagnosis of diaphanospondylodysostosis (DSD): a case report Key Clinical Message.
853 *Clin. Case Reports* **6**, 420–425.

854 **Hottentot, Q. P., Van Min, M., Splinter, E. and White, S. J.** (2017). Targeted locus
855 amplification and next-generation sequencing. In *Methods in Molecular Biology*, pp.
856 185–196. Humana Press Inc.

857 **Hwang, C. H., Keller, J., Renner, C., Ohta, S. and Wu, D. K.** (2019). Genetic interactions
858 support an inhibitory relationship between bone morphogenetic protein 2 and netrin 1
859 during semicircular canal formation. *Development* **146**, dev174748.

860 **Ikeya, M., Kawada, M., Kiyonari, H., Sasai, N., Nakao, K., Furuta, Y. and Sasai, Y.**
861 (2006). Essential pro-Bmp roles of crossveinless 2 in mouse organogenesis.
862 *Development* **133**, 4463–4473.

863 **Ikeya, M., Fukushima, K., Kawada, M., Onishi, S., Furuta, Y., Yonemura, S., Kitamura,
864 T., Nosaka, T. and Sasai, Y.** (2010). Cv2, functioning as a pro-BMP factor via twisted
865 gastrulation, is required for early development of nephron precursors. *Dev. Biol.* **337**,
866 405–414.

867 **Jeong, J., Li, X., McEvilly, R. J., Rosenfeld, M. G., Lufkin, T. and Rubenstein, J. L. R.**
868 (2008). Dlx genes pattern mammalian jaw primordium by regulating both lower jaw-
869 specific and upper jaw-specific genetic programs. *Development* **135**, 2905–2916.

870 **Kawakami, K.** (2007). Tol2: a versatile gene transfer vector in vertebrates. *Genome Biol.* **8
871 Suppl 1**, S7.

872 **Kessels, M. Y., Huitema, L. F. A., Boeren, S., Kranenbarg, S., Schulte-Merker, S., van
873 Leeuwen, J. L. and de Vries, S. C.** (2014). Proteomics Analysis of the Zebrafish
874 Skeletal Extracellular Matrix. *PLoS One* **9**, e90568.

875 **Kettleborough, R. N. W., Busch-Nentwich, E. M., Harvey, S. a, Dooley, C. M., de Bruijn,
876 E., van Eeden, F., Sealy, I., White, R. J., Herd, C., Nijman, I. J., et al.** (2013). A

26

877 systematic genome-wide analysis of zebrafish protein-coding gene function. *Nature*
878 **496**, 494–7.

879 **Kuchinskaya, E., Grigelioniene, G., Hammarsjö, A., Lee, H.-R., Högberg, L.,**
880 **Grigelionis, G., Kim, O.-H., Nishimura, G. and Cho, T.-J.** (2016). Extending the
881 phenotype of BMPER-related skeletal dysplasias to ischiospinal dysostosis. *Orphanet*
882 *J. Rare Dis.* **11**, 1.

883 **Kudoh, T., Tsang, M., Hukriede, N. A., Chen, X., Dedekian, M., Clarke, C. J., Kiang, A.,**
884 **Schultz, S., Epstein, J. A., Toyama, R., et al.** (2001). A gene expression screen in
885 zebrafish embryogenesis. *Genome Res.* **11**, 1979–1987.

886 **Kwon, H. J. and Riley, B. B.** (2009). Mesendodermal signals required for otic induction:
887 Bmp-antagonists cooperate with Fgf and can facilitate formation of ectopic otic tissue.
888 *Dev. Dyn.* **238**, 1582–1594.

889 **Legare, J. M., Seaborg, K., Laffin, J. and Giampietro, P. F.** (2017).
890 Diaphanospondylodysostosis and ischiospinal dysostosis, evidence for one disorder
891 with variable expression in a patient who has survived to age 9 years. *Am. J. Med.*
892 *Genet. Part A* **173**, 2808–2813.

893 **Léger, S. and Brand, M.** (2002). Fgf8 and Fgf3 are required for zebrafish ear placode
894 induction, maintenance and inner ear patterning. *Mech. Dev.* **119**, 91–108.

895 **Li, N., Felber, K., Elks, P., Croucher, P. and Roehl, H. H.** (2009). Tracking gene
896 expression during zebrafish osteoblast differentiation. *Dev. Dyn.* **238**, 459–466.

897 **Lin, Z., Cantos, R., Patente, M. and Wu, D. K.** (2005). Gbx2 is required for the
898 morphogenesis of the mouse inner ear: A downstream candidate of hindbrain signaling.
899 *Development* **132**, 2309–2318.

900 **Liu, Y. G. and Whittier, R. F.** (1995). Thermal asymmetric interlaced PCR: automatable
901 amplification and sequencing of insert end fragments from P1 and YAC clones for
902 chromosome walking. *Genomics* **25**, 674–681.

903 **Lockhart-Cairns, M. P., Lim, K. T. W., Zuk, A., Godwin, A. R. F., Cain, S. A., Sengle, G.**
904 **and Baldock, C.** (2019). Internal cleavage and synergy with twisted gastrulation
905 enhance BMP inhibition by BMPER. *Matrix Biol.* **77**, 73–86.

906 **Maier, E. C. and Whitfield, T. T.** (2014). RA and FGF signalling are required in the
907 zebrafish otic vesicle to pattern and maintain ventral otic identities. *PLoS Genet.* **10**,
908 e1004858.

909 **Mao, H., Li, L., Fan, Q., Angelini, A., Saha, P. K., Wu, H., Ballantyne, C. M., Hartig, S.**
910 **M., Xie, L. and Pi, X.** (2021). Loss of bone morphogenetic protein-binding endothelial
911 regulator causes insulin resistance. *Nat. Commun.* **12**, 1–10.

912 **Merlo, G. R., Paleari, L., Mantero, S., Zerega, B., Adamska, M., Rinkwitz, S., Bober, E.**
913 **and Levi, G.** (2002). The Dlx5 Homeobox Gene Is Essential for Vestibular
914 Morphogenesis in the Mouse Embryo through a BMP4-Mediated Pathway. *Dev. Biol.*
915 **248**, 157–169.

916 **Miller, A. C., Obholzer, N. D., Shah, A. N., Megason, S. G. and Moens, C. B.** (2013).
917 RNA-seq-based mapping and candidate identification of mutations from forward genetic
918 screens. *Genome Res.* **23**, 679–686.

919 **Morsli, H., Choo, D., Ryan, A., Johnson, R. and Wu, D. K.** (1998). Development of the
920 mouse inner ear and origin of its sensory organs. *J. Neurosci.* **18**, 3327–3335.

921 **Moser, M., Yu, Q., Bode, C., Xiong, J. W. and Patterson, C.** (2007). BMPER is a
922 conserved regulator of hematopoietic and vascular development in zebrafish. *J. Mol.*
923 *Cell. Cardiol.* **43**, 243–253.

27

924 **Mowbray, C., Hammerschmidt, M. and Whitfield, T. T.** (2001). Expression of BMP
925   signalling pathway members in the developing zebrafish inner ear and lateral line.
926   *Mech. Dev.* **108**, 179–184.

927 **Nguyen, V. H., Schmid, B., Trout, J., Connors, S. A., Ekker, M. and Mullins, M. C.**
928   (1998). Ventral and lateral regions of the zebrafish gastrula, including the Neural crest
929   progenitors, are established by a bmp2b/swirl pathway of genes. *Dev. Biol.* **199**, 93–
930   110.

931 **O'Connor, M. B., Umulis, D., Othmer, H. G. and Blair, S. S.** (2006). Shaping BMP
932   morphogen gradients in the Drosophila embryo and pupal wing. *Development* **133**,
933   183–193.

934 **Oh, S.-H. H., Johnson, R. and Wu, D. K.** (1996). Differential Expression of Bone
935   Morphogenetic Proteins in the Developing Vestibular and Auditory Sensory Organs. *J.*
936   *Neurosci.* **16**, 6463–6475.

937 **Ohta, S., Mansour, S. L. and Schoenwolf, G. C.** (2010). BMP/SMAD signaling regulates
938   the cell behaviors that drive the initial dorsal-specific regional morphogenesis of the
939   otocyst. *Dev. Biol.* **347**, 369–381.

940 **Ohta, S., Wang, B., Mansour, S. L. and Schoenwolf, G. C.** (2016). BMP regulates regional
941   gene expression in the dorsal otocyst through canonical and non-canonical intracellular
942   pathways. *Dev.* **143**, 2228–2237.

943 **Ohyama, T., Basch, M. L., Mishina, Y., Lyons, K. M., Segil, N. and Groves, A. K.** (2010).
944   BMP signaling is necessary for patterning the sensory and nonsensory regions of the
945   developing mammalian cochlea. *J. Neurosci.* **30**, 15044–15051.

946 **Oxtoby, E. and Jowett, T.** (1993). Cloning of the zebrafish krox-20 gene (krx-20) and its
947   expression during hindbrain development. *Nucleic Acids Res.* **21**, 1087–1095.

948 **Parinov, S., Kondrichin, I., Korzh, V. and Emelyanov, A.** (2004). Tol2 transposon-
949   mediated enhancer trap to identify developmentally regulated zebrafish genes in vivo.
950   *Dev. Dyn.* **231**, 449–459.

951 **Pérez, L. M., de Lucas, B. and Gálvez, B. G.** (2021). BMPER is upregulated in obesity and
952   seems to have a role in pericardial adipose stem cells. *J. Cell. Physiol.* **236**, 132–145.

953 **Radosevic, M., Robert-Moreno, À., Coolen, M., Bally-Cuif, L. and Alsina, B.** (2011).
954   Her9 represses neurogenic fate downstream of Tbx1 and retinoic acid signaling in the
955   inner ear. *Development* **138**, 397–408.

956 **Reichert, S., Randall, R. A. and Hill, C. S.** (2013). A BMP regulatory network controls
957   ectodermal cell fate decisions at the neural plate border. *Dev.* **140**, 4435–4444.

958 **Rentzsch, F., Zhang, J., Kramer, C., Sebald, W. and Hammerschmidt, M.** (2006).
959   Crossveinless 2 is an essential positive feedback regulator of Bmp signaling during
960   zebrafish gastrulation. *Development* **133**, 801–811.

961 **Robledo, R. F. and Lufkin, T.** (2006). Dlx5 and Dlx6 homeobox genes are required for
962   specification of the mammalian vestibular apparatus. *Genesis* **44**, 425–437.

963 **Rodríguez-Aznar, E., Barrallo-Gimeno, A. and Nieto, M. A.** (2013). Scratch2 prevents cell
964   cycle re-entry by repressing miR-25 in postmitotic primary neurons. *Ann. Intern. Med.*
965   **158**, 5095–5105.

966 **Sajan, S. A., Rubenstein, J. L. R., Warchol, M. E. and Lovett, M.** (2011). Identification of
967   direct downstream targets of Dlx5 during early inner ear development. *Hum. Mol.*
968   *Genet.* **20**, 1262–1273.

969 **Schindelin, J., Arganda-Carreras, I., Frise, E., Kaynig, V., Longair, M., Pietzsch, T.,**
970   **Preibisch, S., Rueden, C., Saalfeld, S., Schmid, B., et al.** (2012). Fiji: an open-source

971   platform for biological-image analysis. *Nat. Methods* **9**, 676–82.

972 **Schmid, B., Fürthauer, M., Connors, S. A., Trout, J., Thisse, B., Thisse, C. and Mullins,**
973   **M. C.** (2000). Equivalent genetic roles for bmp7/snailhouse and bmp2b/swirl in
974   dorsoventral pattern formation. *Development* **127**, 957–967.

975 **Scottoline, B., Rosenthal, S., Keisari, R., Kirpekar, R., Angell, C. and Wallerstein, R.**
976   (2012). Long-term survival with diaphanospondylodysostosis (DSD): Survival to 5 years
977   and further phenotypic characteristics. *Am. J. Med. Genet. Part A* **158 A**, 1447–1451.

978 **Serpe, M., Umulis, D., Ralston, A., Chen, J., Olson, D. J., Avanesov, A., Othmer, H.,**
979   **O'Connor, M. B. and Blair, S. S.** (2008). The BMP-Binding Protein Crossveinless 2 Is
980   a Short-Range, Concentration-Dependent, Biphasic Modulator of BMP Signaling in
981   Drosophila. *Dev. Cell* **14**, 940–953.

982 **Shawi, M. and Serluca, F. C.** (2008). Identification of a BMP7 homolog in zebrafish
983   expressed in developing organ systems. *Gene Expr. Patterns* **8**, 369–375.

984 **Solomon, K. S., Kudoh, T., Dawid, I. B. and Fritz, A.** (2003). Zebrafish foxi1 mediates otic
985   placode formation and jaw development. *Development* **130**, 929–940.

986 **Stooke-Vaughan, G. A., Obholzer, N. D., Baxendale, S., Megason, S. G. and Whitfield,**
987   **T. T.** (2015). Otolith tethering in the zebrafish otic vesicle requires Otogelin and α-
988   Tectorin. *Development* **142**, 1137–45.

989 **Sztal, T. E. and Stainier, D. Y. R.** (2020). Transcriptional adaptation: a mechanism
990   underlying genetic robustness. *Development* **147**, dev186452.

991 **Thisse, B. and Thisse, C.** (2004). Fast Release Clones: A High Throughput Expression
992   Analysis. *ZFIN Direct Data Submiss.*

993 **Thisse, C. and Thisse, B.** (2008). High-resolution in situ hybridization to whole-mount
994   zebrafish embryos. *Nat. Protoc.* **3**, 59–69.

995 **Tuazon, F. B. and Mullins, M. C.** (2015). Temporally coordinated signals progressively
996   pattern the anteroposterior and dorsoventral body axes. *Semin. Cell Dev. Biol.* **42**, 118–
997   133.

998 **Urness, L. D., Wang, X., Doan, H., Shumway, N., Noyes, C. A., Gutierrez-Magana, E.,**
999   **Lu, R. and Mansour, S. L.** (2018). Spatial and temporal inhibition of FGFR2b ligands
1000   reveals continuous requirements and novel targets in mouse inner ear morphogenesis.
1001   *Dev.* **145**, dev170142.

1002 **Whitfield, T. T., Granato, M., van Eeden, F. J., Schach, U., Brand, M., Furutani-Seiki, M.,**
1003   **Haffter, P., Hammerschmidt, M., Heisenberg, C. P., Jiang, Y. J., et al.** (1996).
1004   Mutations affecting development of the zebrafish inner ear and lateral line.
1005   *Development* **123**, 241–54.

1006 **Wu, D. K. and Oh, S. H.** (1996). Sensory organ generation in the chick inner ear. *J.*
1007   *Neurosci.* **16**, 6454–6462.

1008 **Zhang, J. L., Huang, Y., Qiu, L. Y., Nickel, J. and Sebald, W.** (2007). Von Willebrand
1009   factor type C domain-containing proteins regulate bone morphogenetic protein signaling
1010   through different recognition mechanisms. *J. Biol. Chem.* **282**, 20002–20014.

1011 **Zhang, J. L., Patterson, L. J., Qiu, L. Y., Graziussi, D., Sebald, W. and Matthias, H.**
1012   (2010). Binding between crossveinless-2 and chordin von willebrand factor type c
1013   domains promotes bmp signaling by blocking chordin activity. *PLoS One* **5**, 1–12.

1014 **Zinski, J., Tuazon, F., Huang, Y., Mullins, M. and Umulis, D.** (2019). Imaging and
1015   quantification of P-Smad1/5 in zebrafish blastula and gastrula embryos. In *Methods in*
1016   *Molecular Biology*, pp. 135–154. Humana Press Inc.

1017 **Zong, Z., Tees, S., Miyanji, F., Fauth, C., Reilly, C., Lopez, E., Tredwell, S., Paul**

1018 **Goldberg, Y., Delaney, A., Eydoux, P., et al.** (2015). BMPER variants associated with
1019 a novel, attenuated subtype of diaphanospondylodysostosis. *J. Hum. Genet.* **60**, 743–
1020 747.

1021

1022

1023 **Figures**

1024
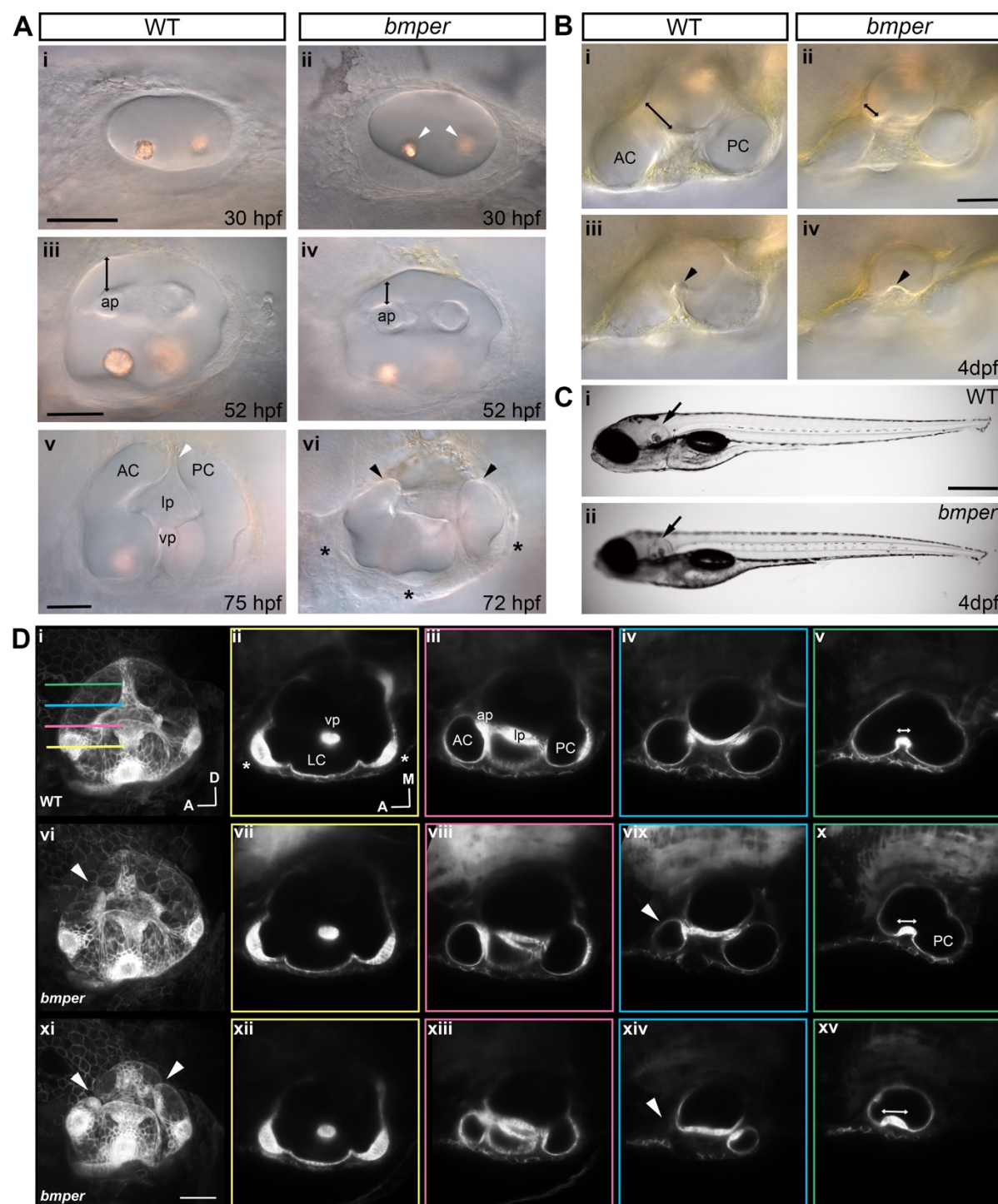
Figure 1. The ears of *bmper* mutant embryos have truncated anterior and posterior semicircular canal ducts.

A (i-vi) Live DIC images of the otic vesicle in phenotypically wild-type (WT) sibling (i, iii, v) and *bmper*[sa108] (ii, iv, vi) embryos, lateral view, anterior to the left. (i, ii) 30 hpf, no clear differences in otic vesicle size or shape are seen, and otoliths form normally in *bmper* mutants (white arrowheads). (iii, iv) 52 hpf, *bmper* mutants have a smaller gap between the

1031 anterior and posterior epithelial pillars that span the vesicle and the dorsal edge of the

1032 vesicle (black lines above anterior pillar). (v, vi) 75 hpf (sibling) and 72 hpf (*bmper*); the

1033 semicircular canal lumens have formed in wild-type sibling embryos (v), and the anterior

1034 (AC) and posterior (PC) canal ducts span the full height of the vesicle, separated by the

1035 dorsolateral septum (DLS, white arrowhead). Note the ventral pillar (vp) can be seen below

1036 the lateral projection (lp). In *bmper* mutants, the anterior and posterior canal ducts are

1037 truncated below the height of the otic vesicle (black arrowheads); the ventral pillar is present

1038 but cannot be seen in this view. All three cristae are present (black asterisks). **B** (i-iv)

1039 Dorsal view of the otic vesicle, anterior to the left, dorsal to the top, at 4 dpf in wild-type

1040 sibling (i, iii) and *bmper* mutant (ii, iv). The wild-type sibling shows clear anterior (AC) and

1041 posterior (PC) canal lumens (i) and a pronounced DLS (black arrowhead, iii), whereas in

1042 *bmper* mutants the anterior canal lumen has a smaller diameter and the length of the

1043 anterior pillar (black line) is shorter than in the wild type (ii); the DLS is also shorter and

1044 wider (black arrowhead). **C** (i, ii) Live DIC image of 4 dpf wild-type sibling (i) and *bmper*

1045 mutant (ii) larvae. Arrows mark the otic vesicle (mis-shapen in *bmper* mutants). Body

1046 length, pigmentation pattern and swim bladder inflation appear normal in *bmper* mutants.

1047 There was no significant difference in body length at 3.5 dpf (two-tailed *t*-test, *p*=0.427,

1048 *n*=29) **D** (i-xv) Light-sheet microscope images using the *Tg(smad6b:GFP)* line, showing a

1049 Maximum Intensity Projection (MIP) lateral view of 4 dpf otic vesicles on the left (i, vi, xi) and

1050 corresponding single *z* slices of a dorsal view through four different planes for each otic

1051 vesicle. (i-v) WT, wild-type sibling, (vi-xv) *bmper* mutant. Each *z* slice is taken at the level

1052 shown by the coloured lines on the WT lateral view (i), such that the *z*-slices in the yellow

1053 boxes (ii, vii, xii), are taken at the lowest ventral plane and the *z*-slices in the green boxes

1054 are taken at the most dorsal plane. The distance between each of the four slices is 26.8 μm

1055 (*z* interval=1.381 μm; sample images are 20 *z* planes apart). vi, xi, lateral views of two

1056 different *bmper* mutants: (vi) has a weaker phenotype with a truncation in the anterior canal

1057 (white arrowhead) and a complete posterior canal; (xi) has a more severe phenotype with

1058 both anterior and posterior truncated canals (white arrowheads). The dorsal views show the

1059 cristae (white asterisks), ventral pillar and lateral canal form normally in both *bmper* otic

1060 vesicles shown (yellow planes); note the more severe *bmper* otic vesicle is slightly smaller

1061 (xi). The next plane (magenta) is at the level of the lateral projection and the anterior pillar in

1062 all four otic vesicles; the lumen of the anterior canal is smaller in both *bmper* mutants (viii,

1063 xiii). The two more dorsal planes (blue, green) clearly show the truncated anterior canal in

1064 both *bmper* mutant ears (white arrowhead, vix, xiv) compared to the wild type (iv). In the

1065 weaker *bmper* phenotype the posterior canal remains intact (x), but the DLS does not

1066 develop normally in either *bmper* mutant (white double-headed arrow).

32

1067   Abbreviations: AC, lumen of anterior semicircular canal; ap, anterior pillar; PC, lumen of

1068   posterior semicircular canal; pp, posterior pillar; vp, ventral pillar; lp, lateral projection; DLS,

1069   dorsal lateral septum; A, anterior; D, dorsal; M, medial, MIP, maximum intensity projection.

1070   Scale bars: 50 µm in Ai, for Aii, Aiii, for Aiv, Av, for Avi; 50 µm in Bii, for Bi; 500 µm in Ci, for

1071   Cii, iii, iv; 50 µm in Dxvi for Di-Dxx.

1072

1073
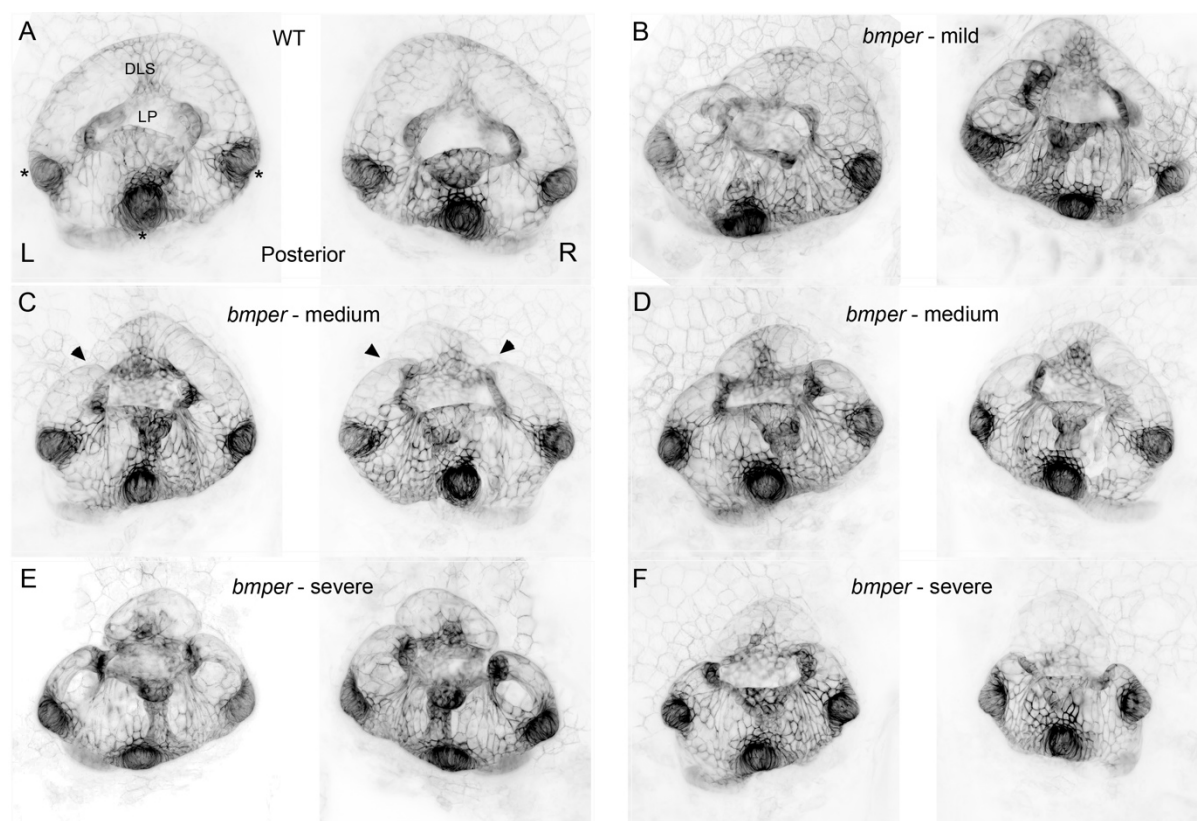
1074

Supplementary Figure S1. The *bmper* mutant phenotype results in variable levels of truncation in the anterior and posterior semicircular canal ducts.

A–F. Light-sheet microscope inverted MIP images of the *Tg(smad6b:EGFP)* line, showing otic vesicles at 5 dpf. Each pair of panels show the left (L) and right (R) ear from the same embryo. The posterior canal is to the centre of each pair of panels. **A**. Wild-type ear showing the position of the DLS, lateral projection (LP) and the strong GFP expression in the cristae (black asterisks). **B–F.** Examples of ears from *bmper*^{sa108} mutants. Variability can be seen between the different ears from the same embryo and also between different embryos. The embryo in B has a milder phenotype with the posterior canal intact on the left ear, compared with the severe phenotypes in D–F, with complete truncations of both semicircular canals in both ears. Truncations are highlighted in panel C (black arrowheads).

A TAIL PCR Method

i

ii

iii

PCR of *Tg(smad6b:EGFP)* DNA using specific genomic primers
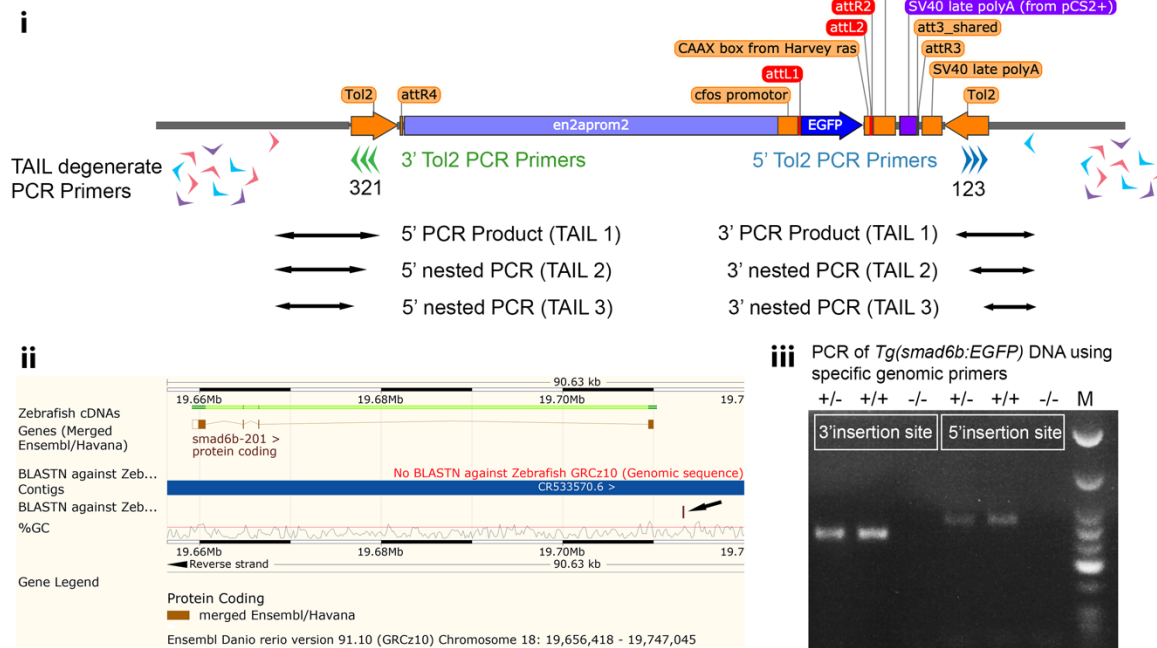
B Targeted Locus Amplification Method

i

Zebrafish protocol

- ○ > 200 somite stage embryos
- ○ Dissociate cells in Ca^{2+}-free Ringers solution
- ○ Remove yolk cells
- ○ Resuspend in dissociation medium
- ○ Count 1×10^7 cells/ml
- ○ Crosslink DNA (Cergentis)
- ○ TLA carried out by Cergentis

ii

Whole genome coverage plot

iii Ch 18 *smad6b*

iv Ch 16 *cysteine-rich venom protein natrin-1-like*

1086

35
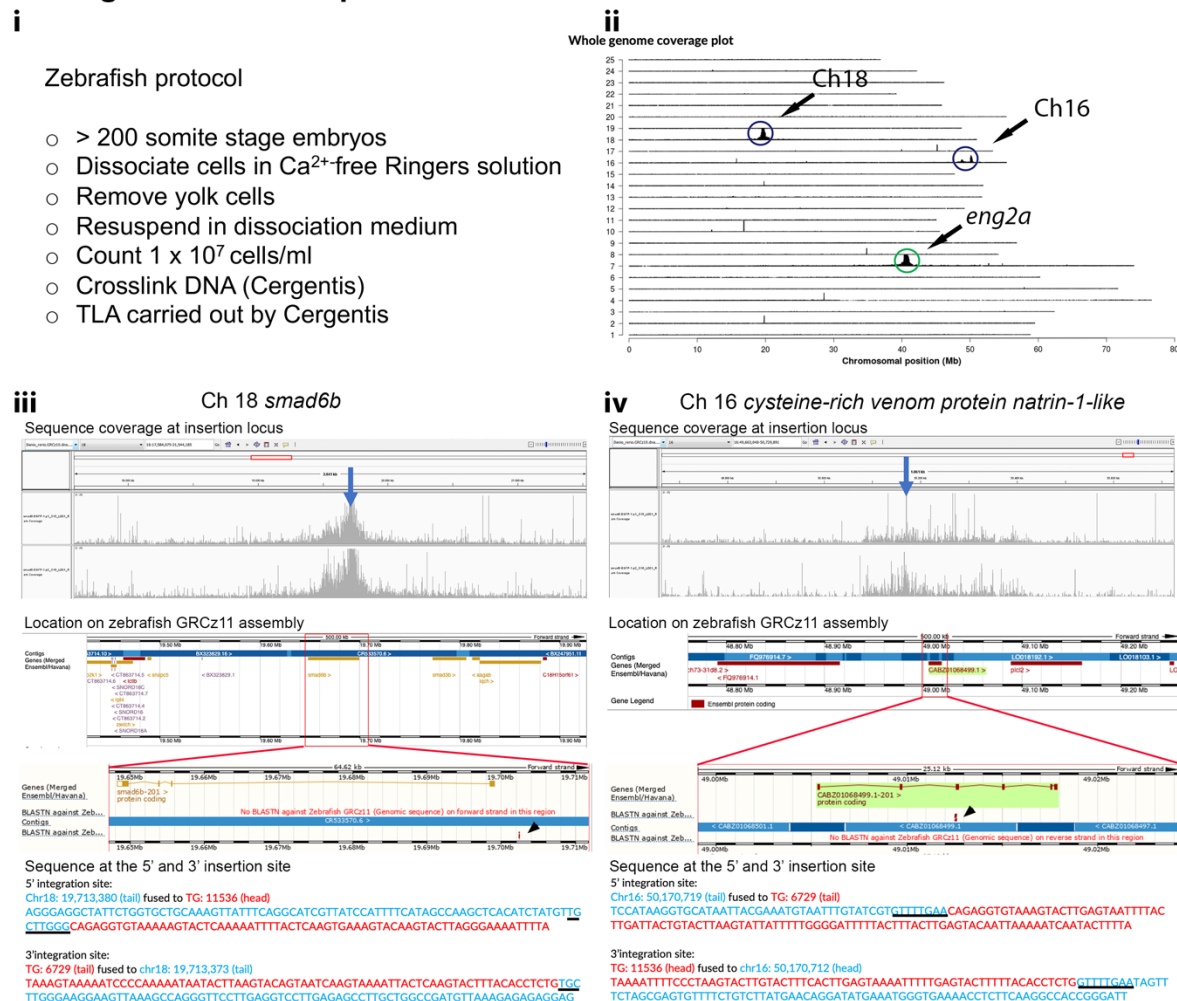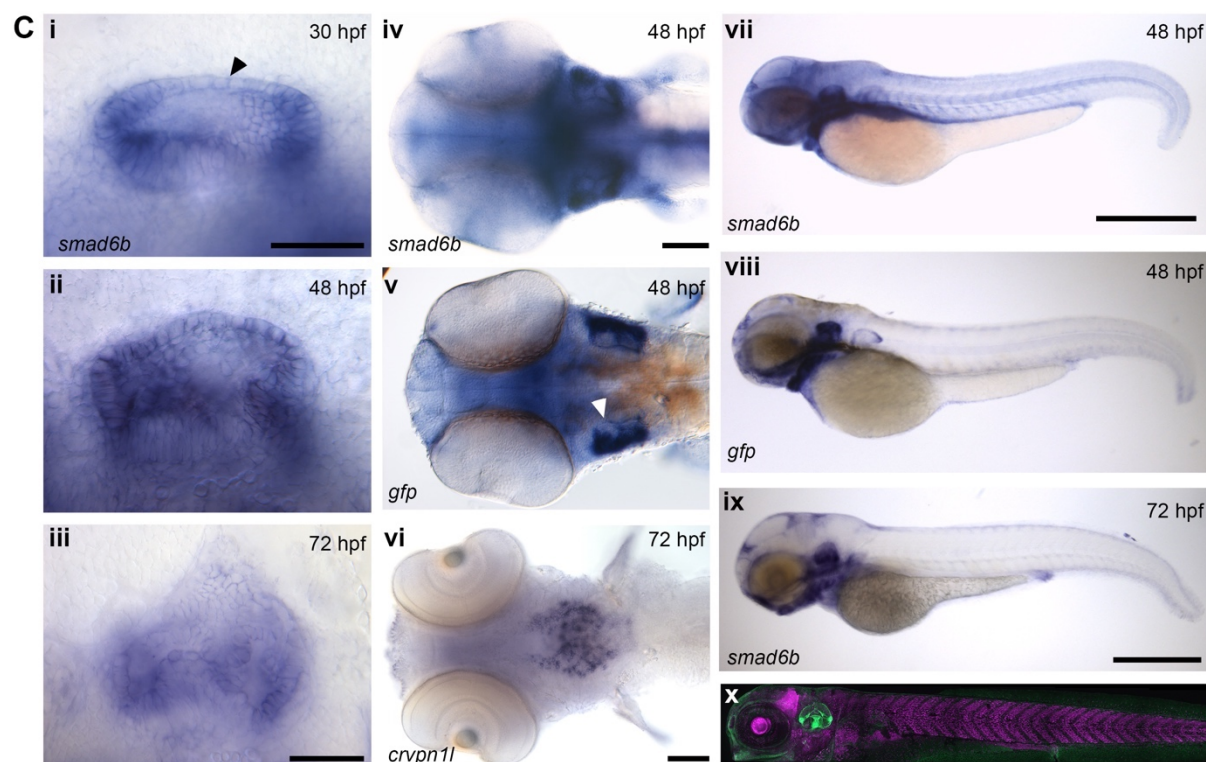
Supplementary Figure S2. Identification of the genomic insertion site of a transgenic line expressing GFP in the inner ear.

A. (i) Overview of the thermal asymmetric interlaced (TAIL-PCR) strategy. Schematic structure of the transgene, containing *engrailed2a* promoter sequences, a *cfos* minimal promoter and EGFP-CAAX coding sequence, flanked by Tol2 sequences. Tol2-specific primers are shown for the 5' (green) and 3' (blue) Tol2 sites. Degenerate primers are shown in red, blue and purple. PCR products from reactions using specific Tol2 primers and degenerate primers are shown. The products from nested PCR reactions (TAIL2 and TAIL3) were used to find flanking genomic sequences. ii PCR products from 5' and 3' reactions that map to the same position in the genome were found to match sequences at the 3' end of the *smad6b* locus. iii The *smad6b* insertion site was confirmed using specific genomic primers and the Tol2-specific primers.

B. (i) Protocol for preparation of zebrafish cell suspension for the Targeted Locus Amplification TLA method. (ii) Result of TLA sequence trace mapping to the zebrafish genome. Peaks can be seen at the same Ch18 locus close to *smad6b* found by TAIL PCR. In addition, another locus on Ch16 was found. The peak on Ch7 in the green circle corresponds to the endogenous *eng2a* locus. (iii) Detailed view of the sequences traces around the insertion site above an overview of the genomic location. Note *smad6b* is also close to *smad3b*. The insertion sequences map to the same 3' region of *smad6b* in the zebrafish GRCz11 assembly. Below is the insertion sequences at the 3' and 5' insertion site.

36

1108   Note the target site duplication (TSD) 8 bp tandem repeated sequence, underlined in black.

1109   iv As in iii for the Ch16 insertion site. The insertion is in the intronic sequence of the

1110   *cysteine-rich venom protein natrin-1-like* gene.

1111   **C.** (i-iii) In situ hybridisation of *smad6b* expression throughout the otic vesicle at i, 30 hpf, ii,

1112   48 hpf, iii, 72 hpf; lateral views, anterior to the left. (iv, v) Dorsal view at 48 hpf of *smad6b*

1113   expression (iv) and *gfp* expression (v), in *Tg(smad6b:EGFP)* embryos, anterior to the left.

1114   *gfp* and *smad6b* mRNA have closely matching spatial expression domains. Note the

1115   expression of *smad6* and *gfp* is weaker more medially and also more dorsally at 30 hpf (i). vi

1116   Ventral view of specific expression of *crvpn1l* at 72 hpf. vii, viii Whole mount in situ staining

1117   of 48 hpf embryos with *smad6b* (vii) and *gfp* (viii) *Tg(smad6b:EGFP)* embryos showing the

1118   overlap in expression. (ix), (x), 72 hpf *Tg*(*smad6b:gfp*) embryos showing strong expression

1119   of *smad6b* in the ear in (ix) and strong otic expression of GFP (green) in a confocal image

1120   (x). Nuclei are labelled with *Tg(Xla.Eef1a1.mRFP1)* (magenta). Scale bars: 50 µm in Ci, for

1121   Cii, Ciii; 100 µm in Civ, for Cv, Cvi; 500 µm in Cvii, for Cviii, Cix.

1122

1123

Supplementary movie 1 – 3D rendered day 7 wild-type sibling ear

3D rendered image of wt 7 dpf otic vesicle using light-sheet images of the *Tg*(*smad6b:EGFP*), line which marks cell membranes of the otic epithelium. The movie begins with a lateral view of the ear with posterior to the left, and as the ear rotates the medial view is seen. The external surface shows the three semicircular canals and the internal view shows the pillars that form the hubs for each canal, the three cristae and the septa that divide the canals.

Supplementary movie 2 – 3D rendered day 7 *bmper* mutant ear

3D rendered image of a *bmper* mutant 7 dpf otic vesicle using light-sheet images of the *Tg(smad6b:EGFP)* line. The movie begins with a lateral view of the ear with posterior to the left, and as the ear rotates the medial view is seen. The external surface shows the three semicircular canals, with a clear truncation in the anterior canal; the posterior canal appears normal. The internal view shows the pillars that form the hubs for each canal, the three cristae and the septa that divide the canals.

Supplementary movie 3 – composite *z* stack movie of wild-type and *bmper* mutant otic vesicles from Figure 1

Movie through the dorsal view of a wild type ear, mild *bmper* and stronger *bmper* phenotype. *z* slices from light-sheet microscopy of the *Tg(smad6b:EGFP)* line. The three embryos from Figure 1D are aligned so that the movie begins at an equivalent depth in each embryo and the semicircular canal truncations in the *bmper* mutants can be seen.

38
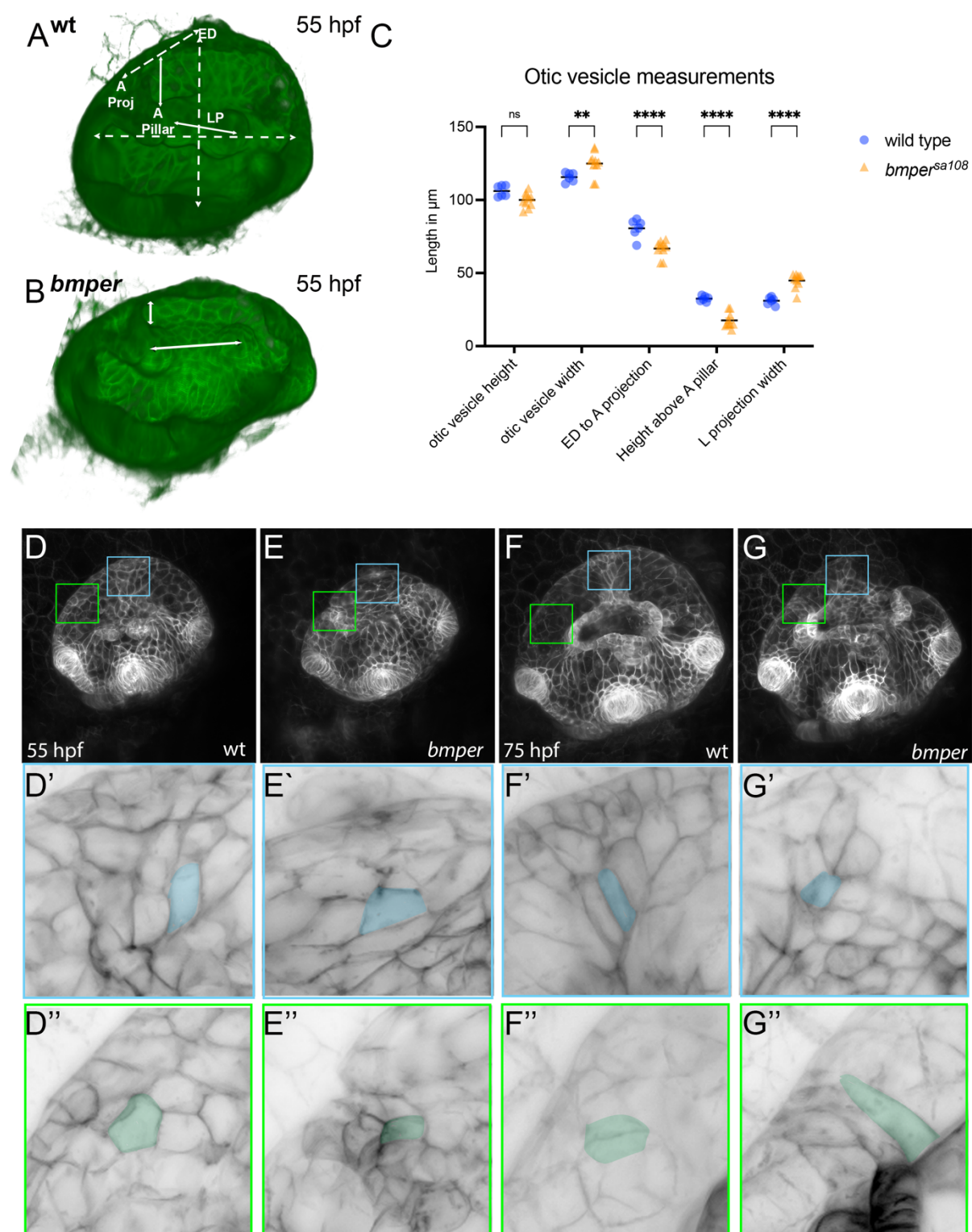
Figure 2. Live fluorescent imaging reveals changes in morphometric measurements and cell shape changes in _bmper^sa108_ embryos.

A–C. Measurements of otic vesicle shape and features in 3D using transparency-rendered images of wild-type (A) and _bmper_ mutant ear (B). _Tg(smad6b:EGFP)_ embryos at 55 hpf taken with light-sheet microscopy. The internal otic vesicle structure is shown viewed from

1153 the medial edge of the ear looking towards the lateral edge, anterior to the left. Positions of

1154 the measurements taken are shown on the wild-type ear (A). White dashed lines correspond

1155 to otic vesicle height, width and the distince from the base of the ED to the base of the

1156 anterior projection. Continuous lines correspond to distance between the anterior pillar

1157 fusion site and the dorsal otic epithelium, and the width of the lateral projection (measured at

1158 the base of the lateral projection on the lateral side of the ear). **C.** Graph of the

1159 measurements in multiple ears for wild type (*n*=6 ears, *N*=3 fish) and *bmper* mutants (*n*=10,

1160 *N*=5). Each ear was imaged twice, from a dorsal and a lateral view, and each point on the

1161 graph represents the average of the two measurements. There were significant differences

1162 in all measurements apart from otic vesicle height. Two-way ANOVA with Šidák's correction

1163 for multiple comparisons: **p=0.0066; ****p<0.0001; ns, not significant. Abbreviations ED,

1164 endolymphatic duct; A, anterior; LP, lateral projection. **D–G''**. Cell shape changes at the

1165 DLS and truncation points. Maximum Intensity Projections (MIPs) of *Tg(smad6b:EGFP)* in

1166 wild-type (D,F) and *bmper* mutant (E,G) ears at 55hpf (D,E) and 75 hpf (F,G). Blue boxes in

1167 D'–G' correspond to the detailed view below of the DLS; green boxes in D''–G'' correspond

1168 to the detailed view of the site of the truncation. Manual segmentation of selected cells,

1169 pseudocoloured blue and green, highlighting the difference in cell shape between wild type

1170 and *bmper*.

1171

1172
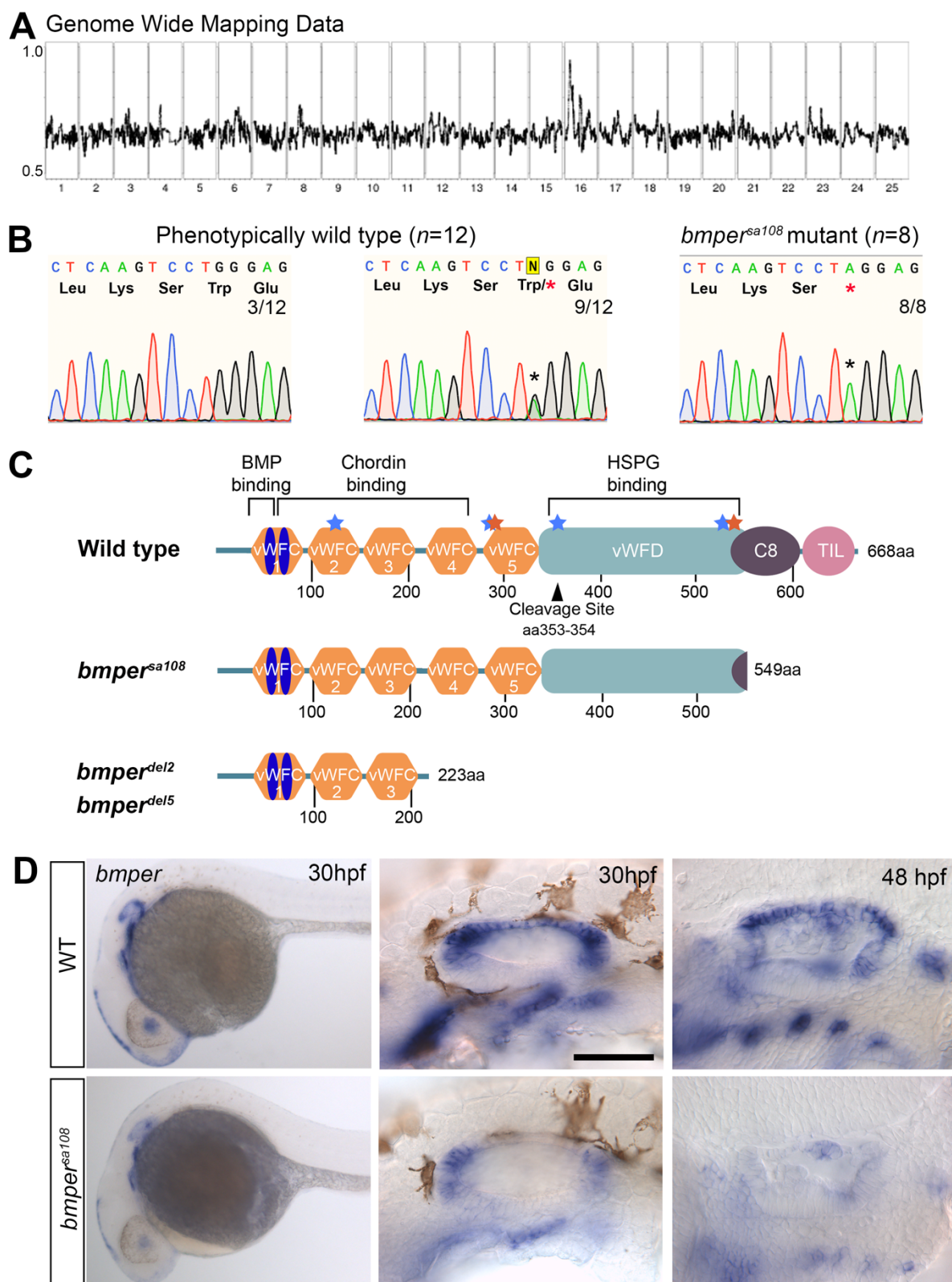
Figure 3. Position of mutations at the *bmper* locus and expression of *bmper* in wild-type and *bmper^sa108^* embryos.

A. RNAseq genome-wide map data showing a strong peak on Chromosome 16. Numbers along the *x* axis indicate chromosomes, 1-25; the *y* axis shows the mutant marker allele

1178   frequency. **B.** Sequence traces from wild-type, heterozygous and homozygous *bmper*

1179   mutant embryos, taken from a *bmper* heterozygous cross. A G>A SNP changes a

1180   Tryptophan residue to a STOP codon in *bmper*^{sa108} mutant embryos. **C.** Schematic of the

1181   zebrafish Bmper protein structure in wild-type and *bmper* mutant alleles. The protein

1182   contains five cysteine-rich von Willebrand factor type C domains (vWFC); a von Willebrand

1183   factor type D domain (vWFD); a cysteine-rich domain (C8), and a trypsin inhibitor-like

1184   domain (TIL). vWFC1 has two sub-domains shown in blue; the N terminal domain is involved

1185   in BMP binding and C terminal domain is part of the chordin-binding domain. The vWFD

1186   domain is suggested to bind to heparan sulphate proteoglycans (HSPG). Positions

1187   corresponding to human disease mutations associated with DSD are shown in blue (V137D,

1188   Q309*, P370L, C546*); mutations associated with the milder condition ISD are shown in

1189   orange (W314*, R558*). Positions are at the homologous position in the zebrafish protein

1190   sequence. Truncations associated with different alleles are shown. **D.** Expression of *bmper*

1191   in the inner ear of wild-type (top row) and *bmper*^{sa108} mutant embryos (bottom row) at 30 hpf,

1192   32 hpf, 48 hpf, anterior to the left. Strong expression can be seen in the dorsal otic vesicle

1193   that is down-regulated. Expression in *bmper*^{sa108} mutant embryos is down-regulated

1194   throughout the embryo (left hand panels); right hand panels show enlargement of the otic

1195   region. Scale bar: 50 μm in view of detailed otic vesicle.

1196

Ai

chromosome num	wt SNPs num	mut SNPs num	wt markers num	corresponding mut markers	left edge	right edge	interval	peak value
1	22897	24763	2188	2081	0	0	0	0.7288
2	23614	25041	1911	1811	0	0	0	0.7176
3	25179	26745	2563	2439	0	0	0	0.7576
4	16527	17253	1260	1168	0	0	0	0.7718
5	27424	28686	2278	2126	0	0	0	0.715
6	21630	22427	2072	1956	0	0	0	0.7632
7	26496	28160	2770	2690	0	0	0	0.7074
8	20145	21329	1671	1597	0	0	0	0.7714
9	17941	19411	1655	1563	0	0	0	0.7038
10	18427	19934	1544	1481	0	0	0	0.7148
11	17681	18853	1709	1609	0	0	0	0.708
12	15143	15787	1386	1106	0	0	0	0.7022
13	19821	21503	1982	1917	0	0	0	0.714
14	15398	16253	1592	1519	0	0	0	0.714
15	17846	18869	1351	1294	0	0	0	0.7244
16	21943	22755	1871	1661	1444165	15420254	13976089	0.9506
17	19605	20719	1386	1311	0	0	0	0.7492
18	16772	17711	1275	1193	0	0	0	0.7518
19	19907	21371	2251	2150	0	0	0	0.697
20	21806	23207	1980	1882	0	0	0	0.7492
21	17016	18861	1772	1705	0	0	0	0.732
22	15927	17158	1120	1069	0	0	0	0.7062
23	18883	19615	1762	1663	0	0	0	0.7654
24	14699	15517	908	863	0	0	0	0.7042
25	16033	17098	1418	1368	0	0	0	0.697

SNP EFFECTS

ii — Predicted Position of the Mutation on Chromosome16

1444165   10101030   15420254

WARNING! Linked ratio was relaxed! Max linkage was 0.9506

Chromosome 16 position

iii HIGH IMPACT

Chromo	Position	Reference	Change	Change_type	Homozygous	Quality	Coverage	Warnings	Gene_ID	Gene_name	Bio_type	Transcript_ID	Exon_ID	Exon_Rank	Effect	old_AA/new_AA	Old/New_codon	Codon_Num(CDS)	Degeneracy	CDS_size
16	8535880	*	+G	INS	Hom	19.3	4	NA	ENSDARG00000076660	FOXO6 (2 of 2)	protein_coding	ENSDART00000112161	exon_16_8535048_8536406	2	FRAME_SHIFT -/?	-/C	318	NA	1785
16	8846347	A	G	SNP	Hom	99.1	7	NA	ENSDARG00000044605	stx12l	protein_coding	ENSDART00000150212	exon_16_8846347_8846452	2	START_LOST M/V	Atg/Gtg	1	1	804
16	8846347	A	G	SNP	Hom	99.1	7	NA	ENSDARG00000044605	stx12l	protein_coding	ENSDART00000065514	exon_16_8846347_8846452	1	START_LOST M/V	Atg/Gtg	1	1	804
16	9261799	C	T	SNP	Hom	200	8	NA	ENSDARG00000040893	bmper	protein_coding	ENSDART00000097348	exon_16_9261751_9262087	12	STOP_GAINED W/*	tGg/tAg	549	1	2004
16	9261799	C	T	SNP	Hom	200	8	NA	ENSDARG00000040893	bmper	protein_coding	ENSDART00000059930	exon_16_9261751_9262087	16	STOP_GAINED W/*	tGg/tAg	545	1	1992
16	11659541	*	+A	INS	Hom	88	7	NA	ENSDARG00000016481	ptpn2a	protein_coding	ENSDART00000104037	exon_16_11659518_11659679	7	FRAME_SHIFT -/?	-/T	279	NA	1170
16	11659541	*	+A	INS	Hom	88	7	NA	ENSDARG00000016481	ptpn2a	protein_coding	ENSDART00000136168	exon_16_11659518_11659679	7	FRAME_SHIFT -/?	-/T	279	NA	1179

B

Allele Name: sa108
Current Status: Available for shipment
Availability: Order Allele From ZIRC
Mutation: G > A
Consequence: Nonsense

Transcript ID	Consequence	Amino Acid Affected	Amino Acid Total	Exon Affected	Exon Total
ENSDART00000059930	Nonsense	545	663	16	20
ENSDART00000097348	Nonsense	549	667	12	16

Genomic Location (Zv9): Chromosome 16 (position 9261799)
Other Location(s):

	Assembly	Chromosome	Position
	GRCz10	16	7243621
	GRCz11	16	7184807

KASP Assay ID: None (used for ordering genotyping assays from LGC Genomics)
KASP Sequence: None
Flanking Sequence: AGTCAAGGTGAAGCTCCGCGCTCACAGAACCTGCCAGAAGCTCAAGTCCT[G/A]GGAGTTTCAGAAGTGCCACTCTGCTGTCGACTTTACCTCCTTTTACAAGT
Associated Phenotype: Normal

C

WT — 5 dpf — *bmper^del2*

D *bmper*

WT — 12S — 18S — 24 hpf — 40 hpf — 50 hpf — 72 hpf

E

bmper WT 48 hpf — *bmper* tbx^-/- 48 hpf — *bmper* WT 28 hpf — *bmper* sox10^-/- 28 hpf

1197

1198 **Supplementary Figure S3**. **Independent confirmation of mutations in *bmper*.**

1199 **A.** (i) RNAseq genome wide-data listing the numbers of wild-type and mutant markers per

1200 chromosome. A strong peak value (0.9506) representing a high mutant marker frequency is

1201 detected on Chromosome 16 at the interval 1444165-15420254. (ii) Graphical view of the

1202 mutant marker frequency at the candidate interval on Ch16. (iii) List of high impact SNPs

1203 and insertions occurring in genes within the candidate interval. A STOP is gained in the

1204 *bmper* gene, making this a strong candidate. **B.** Screenshot from the Sanger Institute

1205 Zebrafish Mutation Project website (sanger.ac.uk/resources/zebrafish/zmp) showing the

1206 *sa108* mutation in the *bmper* gene at the same amino acid residue as the mutation

1207 characterised in Fig. 3. **C.** DIC image of wild-type ear at 5 dpf and the ear in a *bmper^del2^*

1208 mutant, showing truncated anterior and posterior canal ducts (arrowheads). Compare to the

1209 *bmper^sa108^* mutant ear, Fig. 1A(vi). Lateral views, anterior to left. **D.** Expression of the *bmper*

1210 gene in the otic vesicle from 12 somites (12S) to 72 hpf. The strongest dorsal *bmper*

1211 expression is present just prior to the onset of epithelial projection outgrowth (42 hpf

1212 onwards). **E.** Expression of *bmper* in *tbx^-/-^* and *sox10^-/-^* mutant embryos at 48 hpf and 28

1213 hpf, respectively. No difference in the level of expression was detected. Scale bars: 50 µm in

1214 D detailed view of ear; 200 µm in D, 12S whole mount.

1215

1216

1217

1218
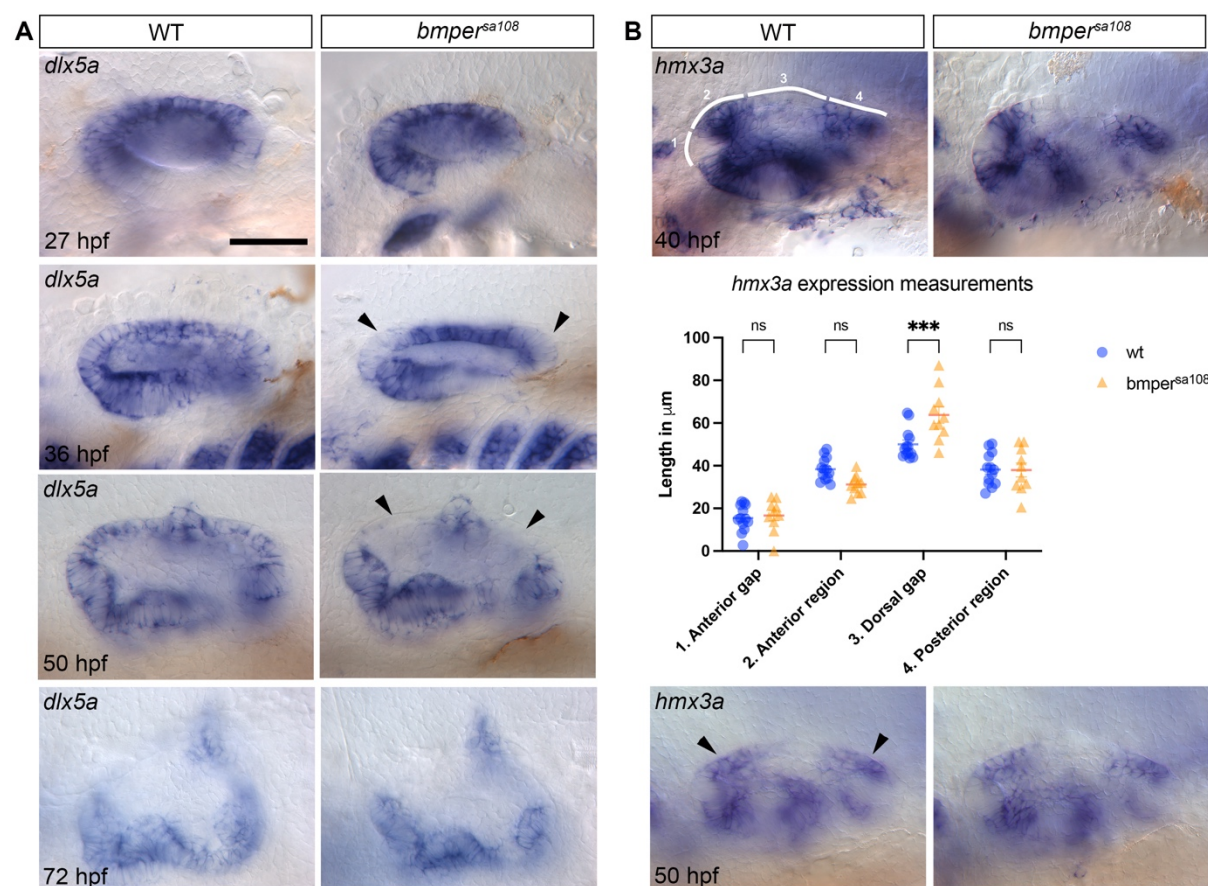
Figure 4. *bmper^sa108* mutants have a specific loss of *dlx5a* in the dorsal otic epithelium and a subtle difference in otic *hmx3a* expression.

A. Lateral view of otic vesicle and *dlx5a* expression in wild-type and *bmper* mutant embryos from 27 hpf to 72 hpf; anterior to the left. Black arrowheads indicate region where expression is absent in *bmper* mutants at 36 and 50 hpf. **B**. Analysis of *hmx3a* expression at 40 hpf and 50 hpf, lateral view of the otic vesicle, anterior to the left. Measurements were taken corresponding to the numbered white lines shown in the image of the wild-type ear at 40 hpf in B. 1. anterior gap; 2, anterior expression; 3, dorsal gap in expression; 4, posterior expression. The data are shown in the graphs below with the corresponding number. Two-way ANOVA with Šidák's correction for multiple comparisons: ***p=0.0003; ns, not significant. Levels of otic *hmx3a* expression appear unaffected, but the dorsal gap in expression increases in size. The region affected overlaps with *bmper* and *dlx5a* expression. Scale bars: 50 µm in A for all images.

1232

1233

1234

45
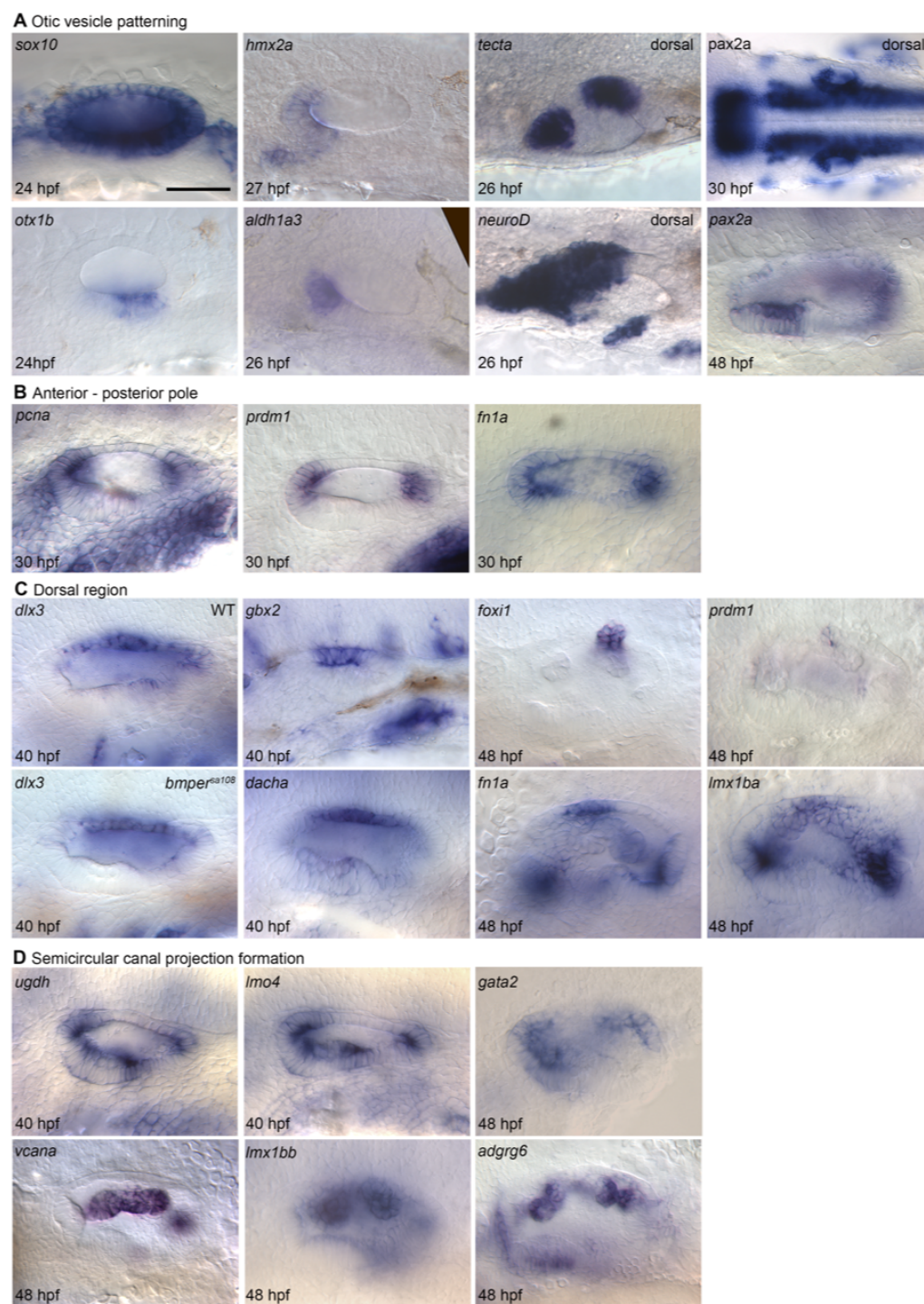
**Supplementary Figure S4. Otic patterning and dorsal gene expression that is unaffected in *bmper^sa108* mutants.**

A. Otic vesicle patterning genes. **B** Genes strongly expressed in the anterior and posterior poles of the otic vesicle are unaffected in *bmper* mutants. **C.** Genes expressed in or around the endolymphatic duct. Note *dlx3* is unchanged in *bmper* mutants, unlike the premature down-regulation of the related gene *dlx5a* (Fig. 4A). **D.** Genes previously shown to be required for semicircular canal morphogenesis are also unaffected in *bmper* mutants. Scale bars: 50 µm in A for all images (except *pax2a* dorsal).
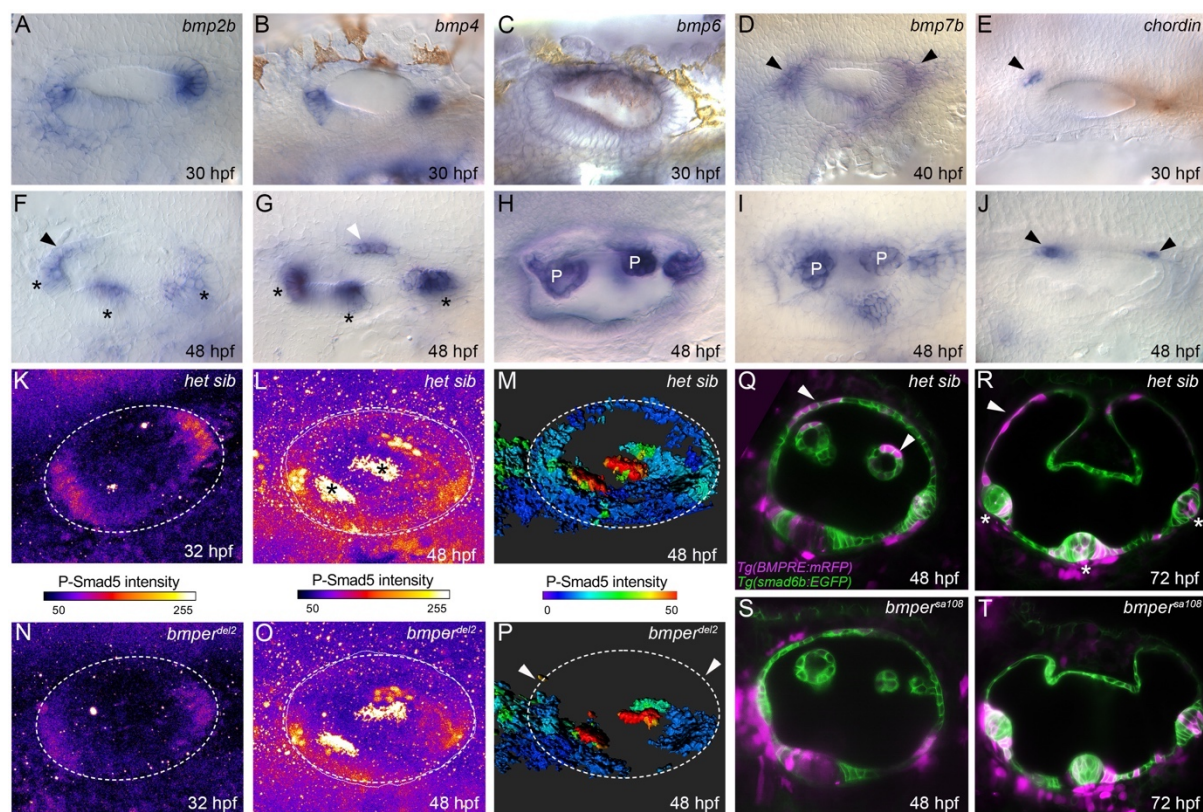
Figure 5. BMP pathway gene signalling is reduced in *bmper^sa108* mutants.

A–J. In situ hybridisations showing no change in the expression of BMP pathway genes in the otic vesicle at 30-40 hpf (A-E) and 48 hpf (F-J). Lateral views; anterior to the left. Expression is seen in the sensory cristae (*bmp2b, bmp4* ,black asterisks, F,G); the lateral dorsal otic epithelium (*bmp2b*, black arrowhead, F); the ED (*bmp4*, white arrowhead, G);the non-sensory epithelial projections (*bmp6*, *bmp7b*, labelled P in H,I); and the periotic mesenchyme (*bmp7b*, *chordin*, black arrowheads, D,E,J). **K-P.** P-Smad5 levels (antibody stain), indicating BMP activity in the otic vesicle at 32 hpf (K,N) and 48 hpf (L,O) in wt (K,L) and MZ *bmper^del2* mutants, lateral view, anterior left. A reduction of activity is seen in the MZ *bmper^del2* otic vesicle at the anterior and posterior poles at 32 hpf. High levels of activity are seen in the sensory maculae at 48 hpf in heterozygous siblings and *bmper^del2* mutants (black asterisks, L). M,P. Relative P-Smad5 levels at 48 hpf show a reduction of P-Smad5 staining in the dorsal otic epithelium (white arrowheads) and a small gap in the ventral otic vesicle (white asterisk). **Q–T.** Expression of the *Tg(BMPRE:mRFP)* reporter line in the *Tg(smad6b:EGFP)* background. mRFP fluorescence corresponding to BMP activity can be seen in phenotypically wild-type embryos in the dorsal otic vesicle at 48 hpf (Q) and 72 hpf (R) and also in the epithelial projections at 48 hpf (white arrowheads) Sensory cristae are shown with white asterisk (R). This expression in non-sensory epithelium is absent in *bmper^sa108* mutant embryos (S,T). Expression in the cristae is unaffected in the mutant ear; expression in periotic mesenchyme appears up-regulated.
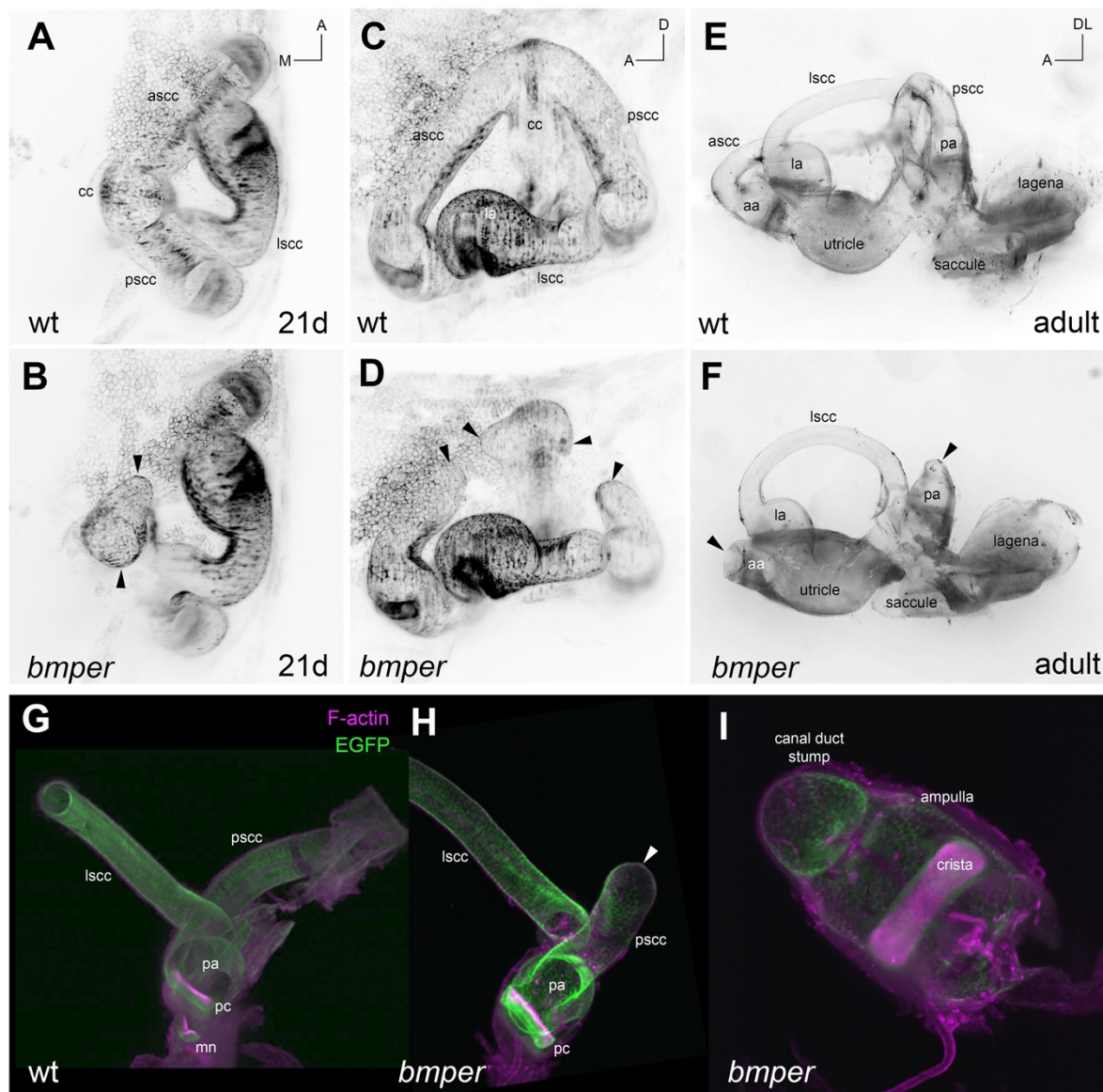
1265

1266
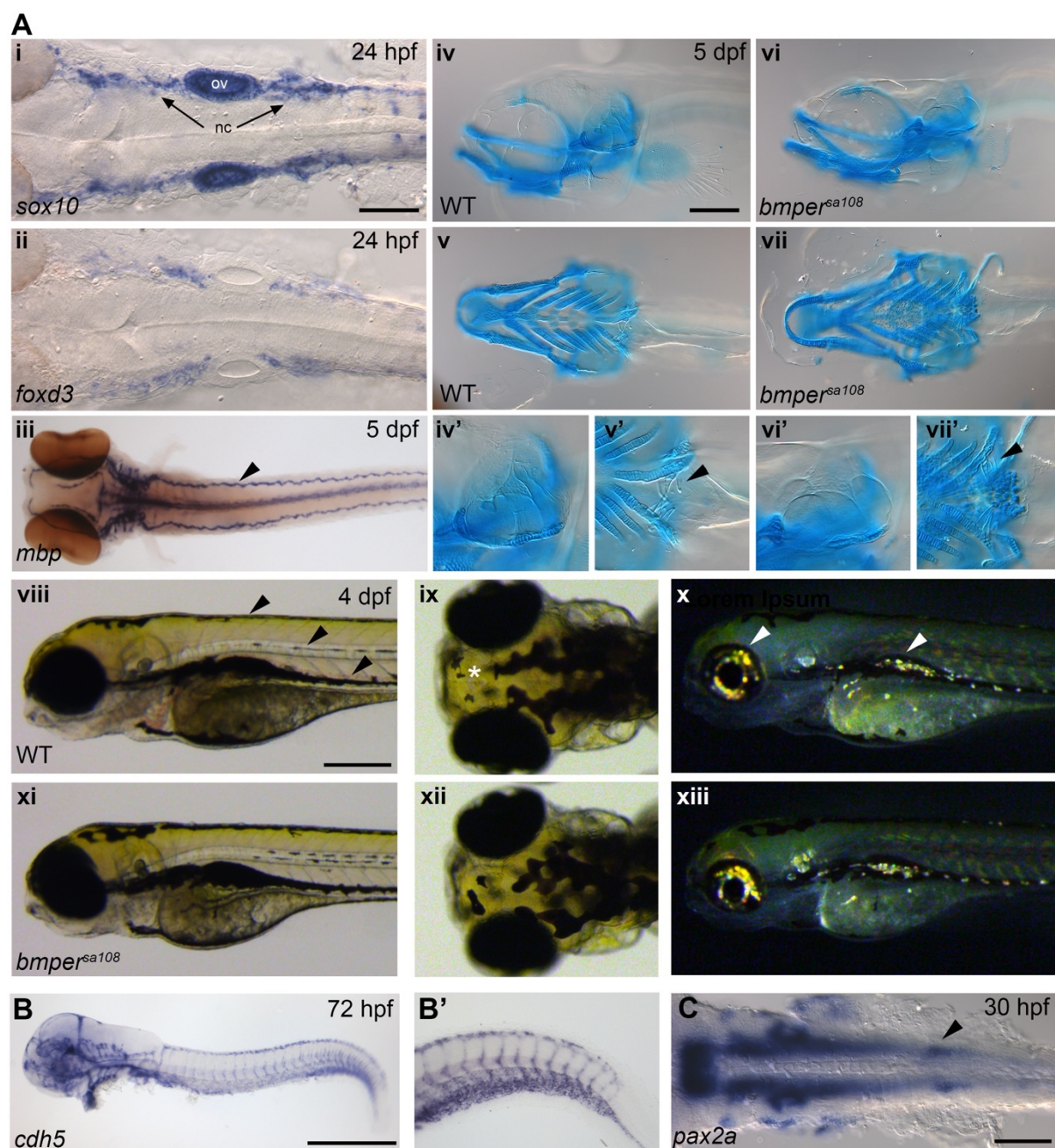
Figure 6. *bmper^sa108* **mutants do not display neural crest, angiogenesis or kidney development defects.**

A. i-ii Dorsal view of 24 hpf embryo showing expression of *sox10* (i) and *foxd3 (*ii). (iii) Dorsal view of 5 dpf larvae showing normal expression of *mbp*. The arrowhead marks expression along the posterior lateral line nerve. (iv-viii) Alcian blue staining of cartilage in wild-type (iv, v) and *bmper* mutant (vi, vii), lateral view (iv, vi) dorsal view (v, vii) iv'-vii' detailed view of panels above showing the structure of the ear in wild-type and *bmper* mutants (black arrowhead)(iv', vi') and the presence of pharyngeal teeth in both wild-type and *bmper* mutant (v', vii')(arrowhead). (viii-xiii) pigmentation is normal in *bmper* mutants (xi-

1276   xiii) as in wild-type, including the normal patterning of three rows of melanocytes in the trunk

1277   (viii, arrowheads), xanthophores (yellow, white asterisk) (ix, xii); and iridophores (white

1278   arrowheads) (x, xiii). **B.** Lateral view of *ve-cadherin* expression at 72 hpf. Expression is

1279   normal in *bmper* mutants; see detail in the tail (B'). **C.** *pax2a* expression in the developing

1280   pronephros (black arrowhead) at 30 hpf is normal. Abbreviations ov, otic vesicle; nc, neural

1281   crest. Scale bars: 100 µm in Ai, for Aii, 200 µm in Aiv, for Av, vi, vii; 500 µm in Aviii, for Ax,

1282   xi, xiii, 500 µm in B; 200 µm in C.

1283

1284

Figure 7. Truncations in the anterior and posterior semicircular canals persist into adulthood in *bmper* mutants.

A-D. Day 21 wild-type (A, C) and *bmper* mutant (B, D) ears expressing the transgene *Tg(smad6b:EGFP)* and imaged using light-sheet microscopy. A,B Dorsal view, anterior to the top, medial to the left. C,D, lateral view, anterior left. **E,F.** Brightfield image of a dissected adult ear from wild-type (E) and *bmper* mutant (F), both dorsal view. Note truncated canals (black arrowhead). The lateral canal is present in *bmper* mutants (F). **G-I.** Fluorescent image of adult *Tg(smad6b:EGFP)* canals, counterstained with TRITC-phalloidin, dissected from wild-type and *bmper* mutant adults. H. Dissected canals from adult *bmper* mutant with a longer truncated posterior canal, compared with example in I (enlarged) where the canal terminated just above the ampulla. Arrowheads mark canal duct truncations. Abbreviations: A, anterior; D, dorsal; DL, dorsolateral; M, medial; cc, crus commune; aa, la, pa, anterior,

1298   lateral and posterior ampullae; pc, posterior crista; ascc, lscc, pscc, anterior, lateral and

1299   posterior semicircular canal ducts; mn, macula neglecta (not included in dissection in H).

1300

51